Lithos 190–191 (2014) 363–382

Contents lists available at ScienceDirect

Lithos

journal homepage: www.elsevier.com/locate/lithos

Petrogenesis of the Late Triassic volcanic rocks in the Southern Yidun arc, SW China: Constraints from the geochronology, geochemistry, and Sr–Nd–Pb–Hf isotopes

Cheng-Biao Leng [a,b,*], Qiu-Yue Huang [b], Xing-Chun Zhang [a,*], Shou-Xu Wang [c], Hong Zhong [a], Rui-Zhong Hu [a], Xian-Wu Bi [a], Jing-Jing Zhu [a], Xin-Song Wang [a,d]

[a] State Key Laboratory of Ore Deposit Geochemistry, Institute of Geochemistry, Chinese Academy of Sciences, Guiyang 550002, China
[b] ARC Centre of Excellence in Ore Deposits, School of Earth Sciences, University of Tasmania, Hobart 7001, Australia
[c] Shandong Gold Group Co. Ltd., Jinan 250014, China
[d] University of Chinese Academy of Sciences, Beijing 100039, China

ARTICLE INFO

Article history:
Received 16 January 2013
Accepted 22 December 2013
Available online 7 January 2014

Keywords:
Zircon U–Pb dating
Sr–Nd–Pb–Hf isotopes
Late Triassic volcanic rocks
Southern Yidun arc
Sanjiang tethyan orogenic belt
Southwest China

ABSTRACT

Studies on zircon ages, petrology, major and trace element geochemistry, and Sr–Nd–Hf–Pb isotopic geochemistry of intermediate volcanic rocks from the Southern Yidun arc, Sanjiang-Tethyan Orogenic Belt, SW China have been undertaken in this paper. They are used to discuss the petrogenesis of these rocks and to constrain the tectonic setting and evolution of the Yidun arc. These intermediate volcanic rocks were erupted at ca. 220 Ma (U–Pb zircon ages). Trachyandesite is the dominant lithology among these volcanic rocks, and is mainly composed of hornblende and plagioclase, with minor clinopyroxene and biotite. A hornblende geobarometer suggests that the stagnation of magma in the lower crust, where plagioclase crystallization was suppressed while hornblende crystallized, giving rise to high Sr/Y ratios that are one of the distinguishing features of adakites, after the primary magma originated from the lithospheric mantle wedge. Steeply right-inclined Rare Earth Element (REE) pattern combined with high La/Yb ratios suggests adakitic affinity of these volcanic rocks, implying that slab-melt from the subducting oceanic crust is a necessary component in the primary magma. Besides, trace element geochemistry and isotopic geochemistry also indicate that partial melting of pelagic sediments in the subduction zone and noticeable contamination with the lower crust were involved in the evolution of parental magma of these volcanic rocks. Based on previous work on the Northern Yidun arc and this study, we propose that the subduction was initiated in the Northern Yidun arc and extended to the southern part and that the Northern Yidun arc is an island arc while the Southern Yidun arc represents a continental arc, probably caused by the existence of the Zhongza Massif, that was invoked to be derived from Yangtze Block, as a possible basement of the Southern Yidun arc.

1. Introduction

The Sanjiang Tethyan Orogenic Belt (STOB) in southwest China is a giant 'jigsaw puzzle' composed of several continental blocks (or terranes), volcanic arcs, and ophiolitic suture zones (Fig. 1a; Jian et al., 2009; Metcalfe, 1996, 2006; Mo et al., 1993; Wang et al., 2000; Zhong, 2000). Previous radiometric investigations of some post-orogenic granite in the Songpan–Garzê Fold belt suggest that the final amalgamation of the STOB probably occurred in the Early Jurassic (e.g., Roger et al., 2010). In this composite orogenic belt, three volcanic island arcs, including the Yidun arc, the Jomda–Weixi arc and the Zaduo–Jinghong arc from east to west, formed due to the subduction of the Paleo-Tethys oceanic slabs (Fig. 1a, Hou et al., 2007; Mo et al., 1993). The Yidun arc, the largest one of the three, is located between the Songpan–Garzê Fold Belt and the Qiangtang Block within the eastern Tibetan Plateau (Reid et al., 2005, 2007; Yin and Harrison, 2000). It is bounded by the Jinshajiang Suture to the west, and the Garzê–Litang Suture to the east (Hou and Mo, 1991; Reid et al., 2007). Meanwhile, the Yidun Arc hosts a significant Cu–Ag–Sn polymetallic mineralization system in the north and a porphyry–skarn Cu polymetallic mineralization system in the south (e.g., Hou et al., 2003, 2007; Leng et al., 2012; Li et al., 2011; Qu et al., 2002; Wang et al., 2011, 2013a,b). The Yidun arc is composed of Triassic volcanic rocks with intercalated flysch that overlies variable Paleozoic metasediments, which formed during the consumption of the Garzê–Litang ocean basin (Hou and Luo, 1992; Hou et al., 2003). Previous studies mainly focused on the tectonic evolution, thermal history and mineralization of the Yidun arc (Hou et al., 2007; Leng et al., 2012; Reid et al., 2005, 2007; Wang et al., 2011, 2013a,b). While much less attention has been paid to the geochemical characteristics and petrogenesis of the Late Triassic volcanic rocks in the arc (Hou and Luo, 1992; Wang et al., 2011, 2013a,b). Hou and Luo (1992) proposed that these

* Corresponding authors at: Institute of Geochemistry, Chinese Academy of Sciences, 46 Guanshui Road, Guiyang 550002, China.
E-mail addresses: lcb8207@163.com (C.-B. Leng), zhangxingchun@vip.gyig.ac.cn (X.-C. Zhang).

0024-4937/$ – see front matter © 2013 Elsevier B.V. All rights reserved.
http://dx.doi.org/10.1016/j.lithos.2013.12.018

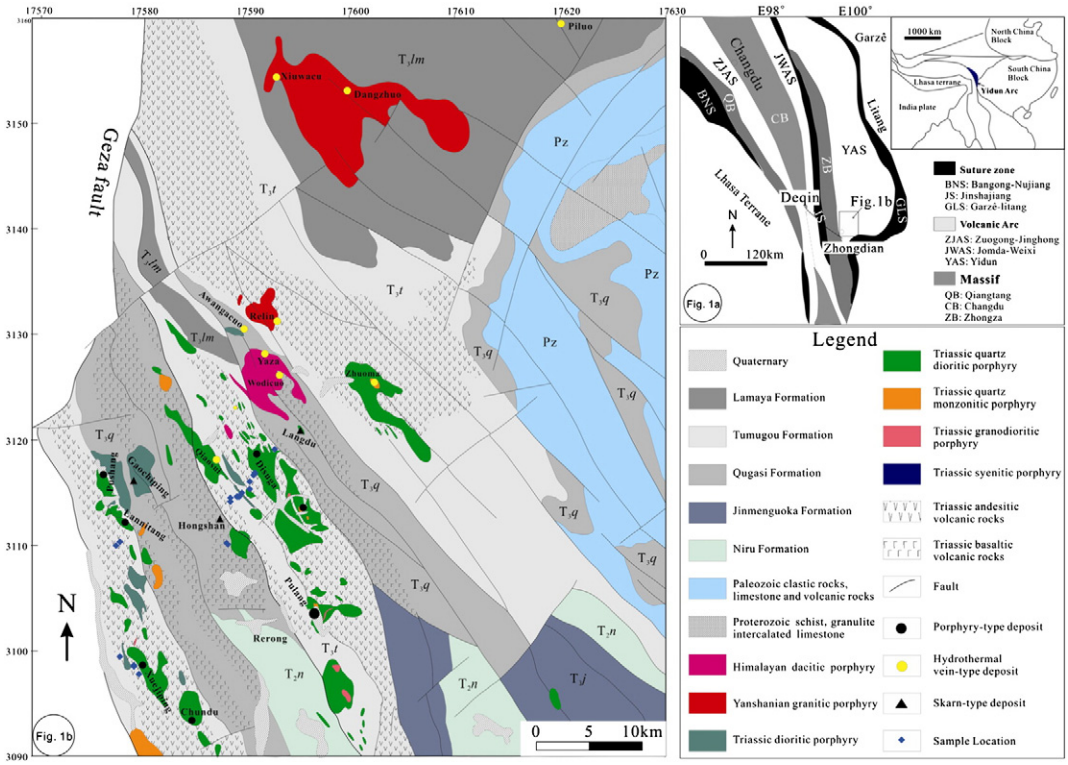

Fig. 1. (a) Location map of the Yidun arc (modified after Mo et al., 1993) and (b) the simplified geological map of the Zhongdian region (modified after Leng et al., 2012), highlighting the Late Triassic volcanic rocks and intermediate-felsic porphyries.

volcanic rocks formed above thin continental crust. It has been suggested that this continental crust could be Proterozoic crystalline basement of the Yangtze Block; though none of Proterozoic strata has been identified yet within the Yidun arc (Chang, 1997). Recently, Wang et al. (2011) noted that Late Triassic volcanic rocks in the Disuga and Xuejiping areas have adakite geochemical signatures (i.e., high Sr/Y and La/Yb ratios), which they suggested as products of partial melting of oceanic slab. Our newly obtained geochemical data for these volcanic rocks in the Southern Yidun arc support this idea. In this paper, we present a suite of new zircon U–Pb ages and in-situ Hf isotopic, Sr–Nd–Pb isotopic, geochemical, and mineralogical data for the Late Triassic volcanic rocks in the Southern Yidun arc (Zhongdian region). This dataset allows us to unravel the petrogenesis of these Late Triassic volcanic rocks and to determine the nature of the magma sources, and to discuss the tectonic and metallogenic implications combined with other published data.

2. Geological setting and samples

The regional geology of the Yidun arc has been described by Reid et al. (2005, 2007), Wang et al. (2011), Leng et al. (2012), and Wang et al. (2013a,b). Tectonically, the Yidun arc is located between the Songpan–Garzê Fold Belt and the Qiangtang Block. It covers a huge area in a "bean-pod" shape with length of 500 km from the Dege County in Sichuan Province to the Shangri-la (Zhongdian) County in Yunnan Province, and a width of 90–160 km. To the east, it is bounded by the Garzê–Litang suture, which is considered to be a Paleotethys oceanic subduction zone dipping to the west during the Middle–Late Triassic. To the west, it is bounded by the Jinshajiang suture, which is considered to be a Late Paleozoic Paleotethys oceanic subduction zone dipping either to the west (Chen et al., 1987; Li et al., 1999; Sengör, 1985; Wang et al., 2000; Zhong, 2000) or to the east (Reid et al., 2005).

The oldest rocks exposed in the Yidun arc are Paleozoic metasedimentary rocks in the Zhongza Massif. These carbonate-rich Paleozoic successions have fossil assemblages similar to sediments and metasediments of the Longmen Shan Thrust Nappe Belt, west of the Yangtze Block (Chang, 1997). It is thus invoked that the Zhongza Massif was separated from the Yangtze Block due to the opening of the Garzê–Litang Ocean during the Middle to Late Palaeozoic, possibly associated with a major Permian phase regional extension (Song et al., 2004; Zhang et al., 1998). The Paleozoic metasediments of the Zhongza Massif were separated from the Triassic cover sequences of the Qiangtang Block to the west by the Jinshajiang Suture, which is interpreted to have been closed in the Middle Triassic (e.g., Wang et al., 2000; Zhong, 2000; Zi et al., 2012). Triassic sequences of clastic rocks intercalating with arc volcanic rocks overlie the Paleozoic sequences of the Yidun arc. The arc volcanic rocks formed during the westward subduction of the Garzê–Litang Ocean in Late Triassic (Chen et al., 1987; Hou, 1993; Hou and Mo, 1991). Jurassic and Cretaceous sediments are absent in the Yidun arc, though there is a belt of Cretaceous granites in its eastern part (Qu et al., 2002; Reid et al., 2007). The Yidun arc was deformed due to the Indosinian orogeny as a consequence of the termination of accretion of the Qiangtang Block to the southern margin of the Eurasian plate during the Late Triassic to Jurassic (e.g., Burchfiel et al., 1995; Reid et al., 2005, 2007; Roger et al., 2010; Xu et al., 1992; Zhou and Graham, 1996). Following the collision of the Indian plate to the Eurasian plate in the Tertiary, the Yidun arc was incorporated into the modern Tibetan Plateau and was deformed by numerous strike-slip faults (Wang and Burchfiel, 2000).

In the Northern Yidun arc (the Changtai arc), widespread Late Triassic bimodal volcanic suites and arc-type volcanic rocks host multiple sulfide deposits (Hou et al., 2003), including the Gacun large Ag-polymetallic VMS deposit and some small Ag–Pb–Zn deposits or occurrences (Hou and Mo, 1991). In the Southern Yidun arc (the Zhongdian arc), numerous Late Triassic intermediate-felsic porphyry bodies, which were emplaced into the contemporaneous volcanic–sedimentary rocks, contain several porphyry-type or skarn-type Cu-polymetallic deposits (Fig. 1b, Leng et al., 2012; Ren et al., 2001; Zeng et al., 2003). Based on the distribution of those porphyry bodies in the Southern Yidun arc, the East and West porphyry belts, bordered by the

Hongshan–Rerong fault, have been roughly delineated (YBGMR, 1990; Zeng et al., 2003). The East porphyry belt mainly comprises the Pulang, Songnuo, Disuga and Qiansui hypabyssal intrusive complexes. The West porphyry belt comprises the Lannitang, Xuejiping, and Chundu hypabyssal intrusive complexes (Fig. 1b).

As stated above, the Southern Yidun arc is composed almost exclusively of Middle and Late Triassic clastic and volcanic rocks. The Late Triassic volcanic–sedimentary sequences were subsequently divided to the Qugasi Formation (T_3q), Tumugou Formation (T_3t) and Lamaya Formation (T_3lm) from the bottom to the top (YBGMR, 1990) (Figs. 1b, 2). The volcanic rocks are predominately developed in the Qugasi and Tumugou Formations. Volcanic rocks of the Qugasi Formation consist of 409-m-thick major massive basalt and minor andesitic volcanic breccia in the lower part and 109-m-thick altered basalt, tuffaceous basalt, and basaltic volcanic breccia in the upper part (Hou et al., 2003). The Tumugou Formation contains over 2500-m-thick volcanic rocks, including major trachyandesite, and minor alkali basalt and dacite, with well-developed columnar joints (Fig. 3b). Both autoliths and crustal xenoliths occur in the intrusive rocks including granodiorite, dioritic porphyry and metagabbro.

The alkali basalt generally contains less than 15 vol.% phenocrysts, which consist mainly of plagioclase (5–10 vol.%), clinopyroxene (0–5 vol.%) or amphibole (0–5 vol.%), with aphanitic or vitrophyric textures (Fig. 3c, d), while, the trachyandesite contains about 20–40 vol.% phenocrysts, which consist mainly of plagioclase (10–20 vol.%), amphibole (5–15 vol.%), biotite (0–5 vol.%) or quartz (0–5 vol.%) with porphyritic texture (Fig. 3d). The accessory minerals include zircon, apatite, magnetite and rutile. These volcanic rocks have generally undergone propylitic or chloritic alterations to various degrees. After petrographic examinations, forty five samples of the least-altered volcanic rocks from the Qugasi and Tumugou Formations in the Zhongdian area have been selected for analyzing whole-rock major and trace element compositions in this study (Sampling locations are shown in Fig. 1b).

3. Analytical methods

3.1. Zircon U–Pb dating methods

The zircons applied for SIMS (Secondary Ion Mass Spectrometry) and LA–ICP-MS (Laser Ablation Inductively Coupled Plasma Mass Spectrometry) U–Pb dating were separated by using conventional heavy liquid and magnetic separation techniques, and then handpicked under a binocular microscope. All zircon grains were documented with micrographs and cathodoluminescence (CL) images to reveal their external and internal structures. Micrographs were taken under transmitted and reflected light microscopes at the State Key Laboratory of Ore Deposit Geochemistry (SKLODG), Institute of Geochemistry, Chinese Academy of Sciences, whereas CL images were obtained by using a microprobe associated instrument JEOL JXA-8900RL at the Institute of Geology, Chinese Academy of Geological Sciences, Beijing, and the mount was vacuum-coated with high-purity gold.

Zircon grains from two samples (DSG07-7, DSG07-3) together with zircon standard Plešovice and Qinghu were mounted in epoxy mounts which were then polished to section the crystals in half for analysis. The analysis of zircon U–Pb isotopic compositions and U, Th and Pb concentrations was conducted by using Cameca IMS 1280 SIMS at the Institute of Geology and Geophysics, Chinese Academy of Sciences in Beijing (IGGCAS). The analytical procedures are described by Li et al. (2009). Measured compositions were corrected for common Pb using the measured non-radiogenic ^{204}Pb. Uncertainties on individual analysis are reported at 1σ level, and weighted mean ages for pooled U–Pb analyses are quoted with 95% confidence interval.

The zircons from other two samples (DSG07-5, HN11-4) were analyzed by using LA–ICP-MS at the State Key Laboratory of Geological Processes and Mineral Resources, China University of Geosciences (Wuhan), and the SKLODG, respectively. Detailed operating conditions for the laser ablation system and the ICP-MS instrument and data reduction are similar to those described by Liu et al. (2008, 2010a,b). Laser sampling was performed using a GeoLas 2005 system. An Agilent 7500a ICP-MS instrument was used to acquire ion-signal intensities. Off-line selection and integration of background and analytic signals,

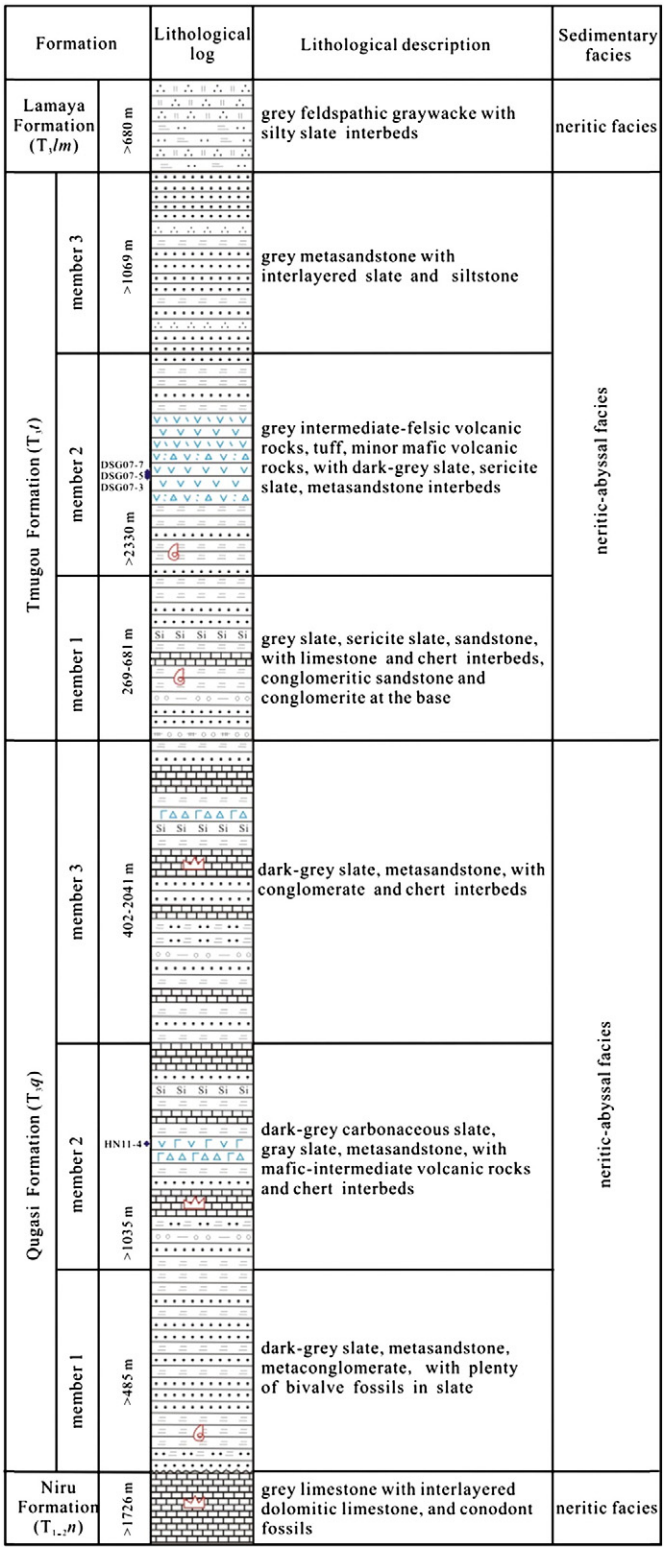

Fig. 2. Late Triassic sedimentary-volcano sequences of the Southern Yidun arc (modified after YBGMR, 1990, 1999; not in scale), showing main lithology and distribution of the analyzed samples.

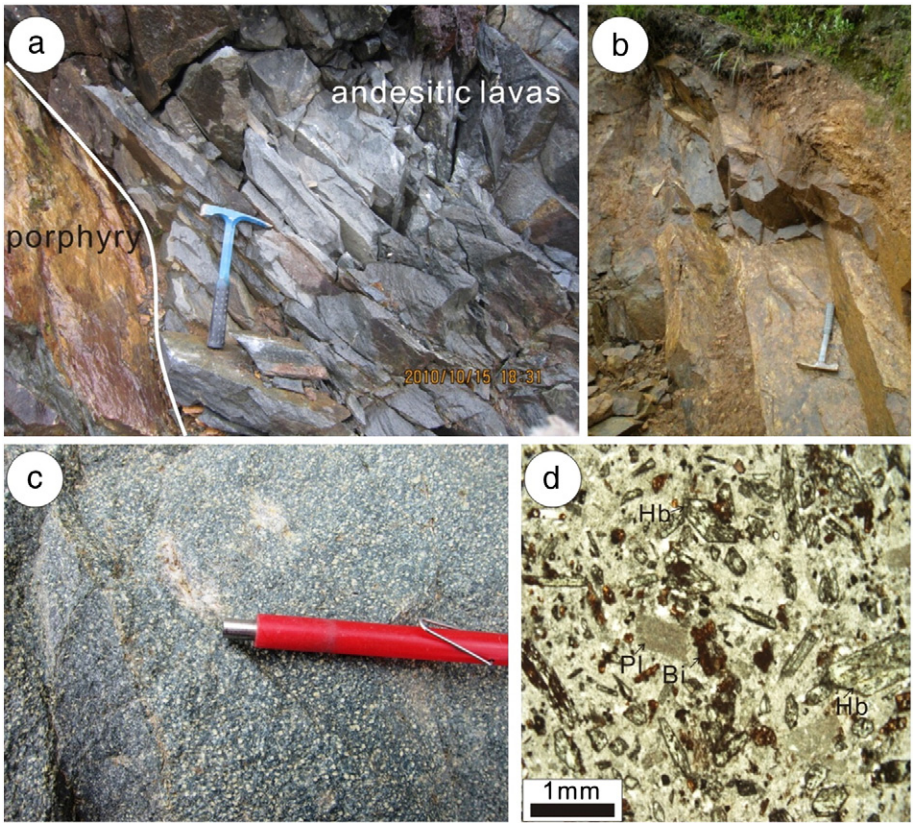

Fig. 3. Field photos and microphotographs of some Late Triassic volcanic rocks in the Southern Yidun arc. a) The outcropped layers of the andesitic lavas that is intruded by the quartz diorite porphyry at the Disuga district; b) the columnar joints of andesitic lavas in the Xuejiping district; c) a hand specimen of trachyandesite at Disuga; d) hornblende (Hb), biotite (Bi), and plagioclase (Pl) phenocrysts in a trachyandesite sample.

and time-drift correction and quantitative calibration for trace element analyses and U–Pb dating were performed by ICPMSDataCal (Liu et al., 2008, 2010a). Zircon 91500 was used as external standard for U–Pb dating, and was analyzed twice every 5 analyses. Preferred U–Th–Pb isotopic ratios used for Zircon 91500 are from Wiedenbeck et al. (1995). Uncertainty of preferred values for the external standard Zircon 91500 is propagated to the ultimate results of the samples. Concordia diagrams and weighted mean calculations are made by using Isoplot/Ex_ver4 (Ludwig, 2003).

3.2. In-situ zircon Hf analysis

In situ zircon Lu–Hf isotopic analyses were undertaken on the same spots, where those were previously dated by SIMS, using a Neptune multi-collector ICP-MS equipped with a Geolas-193 laser-ablation system at the IGGCAS. The detailed instrumental conditions and analytical procedures were described by Wu et al. (2006). In this course, a weighted mean $^{176}Hf/^{177}Hf$ ratio of 0.282516 ± 5 (2σ) has been yielded for the standard Zircon Mud Tank. This is in good agreement with the respectively reported $^{176}Hf/^{177}Hf$ ratios of 0.282507 ± 6 (2σ) from the solution analysis by Woodhead and Hergt (2005) and of 0.282523 ± 43 (2σ) from the in situ analysis by Grifin et al. (2006). Initial Hf isotopic ratios are calculated with reference to the chondritic reservoir at the time of magma crystallization that corresponds to the age of zircon growth from magma. A decay constant of 1.865×10^{-11} $year^{-1}$ for ^{176}Lu (Scherer et al., 2001), and the chondritic ratios of $^{176}Hf/^{177}Hf$ (0.282772) and $^{176}Lu/^{177}Hf$ (0.0332) by Blichert-Toft and Albarede (1997) have been adopted in this study. These values were reported relative to the $^{176}Hf/^{177}Hf$ ratio of 0.282163 for the JMC475 standard. Single stage model ages (T_{DM1}) are calculated using the measured $^{176}Lu/^{177}Hf$ ratios, referring to a model of depleted mantle with a present-day $^{176}Hf/^{177}Hf$ ratio of 0.28325, similar to that of average MORB (Nowell et al., 1998), and $^{176}Lu/^{177}Hf$ ratio of 0.0384 (Griffin et al., 2002). This is similar, though not identical, to the depleted mantle curve defined by juvenile rocks through time (Vervoort and Blichert-Toft, 1999). Two-stage model ages (T_{DM2}) are calculated for the source rock of the magma by assuming a mean $^{176}Lu/^{177}Hf$ value of 0.015 for the average continental crust (Griffin et al., 2002).

3.3. Mineral composition analyses

As the Zhongdian volcanic rocks have experienced hydrothermal alteration in various degrees, only several phenocryst populations were chosen to analyze their chemical compositions by using wavelength-dispersive X-ray analysis on an EPMA-1600 electron probe at the SKLODG. Standard operating conditions include 25 kV for accelerating voltage, 10 nA for specimen current, and 10 μm for beam diameter. SPI mineral standards (USA) were used for calibration.

3.4. Major, trace element and Sr–Nd–Pb analyses

Major oxides of the samples were measured by using an X-ray fluorescence spectrometer (XRF) on fused glass beads at the ALS Chemex (Guangzhou) Co., Ltd. Trace elements were mostly analyzed by using inductively coupled plasma mass spectrometry (ICP-MS) at the SKLODG following the procedures of Qi et al. (2000). In order to check the accuracy of the analyses, some samples including two duplicates were sent to the ALS Chemex (Guangzhou) Co. Ltd. for double checking. The analytical results of trace elements for the double check in samples agree well. The analytical precision and accuracy for most trace elements measured are generally better than 5%.

The whole-rock Sr–Nd–Pb isotopic analyses were performed on an IsoProbe-T Thermal Ionization Mass Spectrometer (TIMS) at Analytical

Laboratory, Beijing Research Institute of Uranium Geology. The mass fractionation corrections for Sr and Nd isotopic ratios are based on the $^{86}Sr/^{88}Sr$ ratio of 0.1194 and $^{146}Nd/^{144}Nd$ ratio of 0.7219, respectively. The $^{87}Sr/^{86}Sr$ ratio of the Standard NBS987 and $^{143}Nd/^{144}Nd$ ratio of the Standard SHINESTU determined in this study were 0.710250 ± 0.000007 (2σ) and 0.512118 ± 0.000003 (2σ), respectively. The $^{208}Pb/^{206}Pb$, $^{207}Pb/^{206}Pb$ and $^{204}Pb/^{206}Pb$ ratios of the Standard NBS981 measured in this study were 2.1681 ± 0.0008 (2σ), 0.91464 ± 0.00033 (2σ) and 0.059042 ± 0.000037 (2σ), respectively.

4. Results

4.1. U–Pb zircon geochronology

Three samples (DSG07-7, DSG07-5, and DSG07-3) from the Tumugou Formation and one sample (HN11-4) from the Qugasi Formation have been dated in this study (Tables 1 and 2). Most zircon grains are subhedral to euhedral, and transparent to light brown. In addition, most zircon grains, with the exception of few grains, show clear igneous oscillatory or planar growth zonation in their CL images (Fig. 4).

A concordia age of 219.8 ± 1.9 Ma (2σ, MSWD = 0.15; Table 1 and Fig. 5a) has been taken as the best estimate of the formation age of the sample DSG07-7 based on 13 out of 14 analytical results analyzed on 14 zircon grains by using SIMS. However, a $^{206}Pb/^{238}U$ age of 1778 ± 25 Ma, which is much older than the above concordia age, is obtained for one zircon grain (spot 3) which is interpreted to represent an inherited zircon grain. 17 zircon grains from the sample DSG07-3 were analyzed by using SIMS. A scatter of mostly concordant ages, ranging from Proterozoic to Mesozoic (Table 1; Fig. 5c), has been yielded. The $^{206}Pb/^{238}U$ ages vary from 209.1 ± 3.1 Ma to 223.5 ± 3.3 Ma for 5 zircon grains (spots 6, 8, 12, 14, 15) with igneous oscillatory zonation in their CL images, with a concordia age of 218.1 ± 4.8 Ma (2σ, MSWD = 2.0). This concordia age of 218.1 ± 4.8 Ma is considered to represent the formation age of the sample DSG07-3. Other concordant ages ranging from 252 Ma to 1943 Ma for 12 zircon grains are interpreted to represent crystalline ages of 12 inherited zircons. There is a large range of $^{206}Pb/^{238}U$ ages for 22 analyzed zircon grains from the sample DSG07-5 (Table 2; Fig. 5d). 10 out of 22 $^{206}Pb/^{238}U$ ages vary from 196 ± 2 Ma to 232 ± 3 Ma, with a weighted mean age of 220.8 ± 5.3 Ma (2σ, MSWD = 5.8). The $^{206}Pb/^{238}U$ ages for other 12 zircon grains from the sample DSG07-5 vary from 253 Ma to 2589 Ma. Their significance will be discussed below.

22 zircon grains from the sample HN11-4 collected from the Qugasi Formation were analyzed (Table 2; Fig. 5b). Their $^{206}Pb/^{238}U$ ages vary from 208 ± 3 Ma to 236 ± 4 Ma, with a weighted mean age of 219.1 ± 3.2 Ma (MSWD = 5.3, 95% confidence interval), which is interpreted to be the crystallization age of this sample.

4.2. In-situ Hf isotopes of zircon

The Lu–Hf isotopes were analyzed on the same domains of zircon grains, which were previously dated by the U–Pb SIMS method, of the above two samples (DSG07-7, DSG07-3), and the results are listed in Table 3. The initial Hf ratios of all analyzed zircon spots were calculated at t = 220 Ma for comparison.

12 analyses were made for 12 zircon grains from the sample DSG07-7. The calculated $\varepsilon_{Hf}(t)$ values of 11 analyses vary from 0.9 to 4.1 with an average of 2.2. Their corresponding single-stage Hf model ages (T_{DM1})

Table 1
SIMS zircon U–Pb data of DSG07-7 and DSG07-3 in the Southern Yidun.

Spots	U	Th	Th/U	$^{207}Pb/^{206}Pb$		$^{207}Pb/^{235}U$		$^{206}Pb/^{238}U$		ρ	$^{207}Pb/^{206}Pb$		$^{207}Pb/^{235}U$		$^{206}Pb/^{238}U$		f_{206} %	Concordance
	ppm	ppm		Ratio	±1σ(%)	Ratio	±1σ(%)	Ratio	±1σ(%)		Age	±1σ	Age	±1σ	Age	±1σ		
DSG07-7 (basaltic andesite)																		
01	108	132	1.22	0.12288	2.84	0.23628	3.28	0.0350	1.60	0.48715	144.6	65.9	215.4	6.4	221.9	3.5	0.69	97%
02	277	451	1.63	0.06920	0.66	0.24061	2.65	0.0346	1.51	0.56738	212.9	49.9	218.9	5.2	219.5	3.3	0.10	100%
03	78	90	1.16	0.05012	1.62	4.75132	1.78	0.3177	1.60	0.89602	1774.1	14.4	1776.3	15.1	1778.3	24.9	0.04	100%
04	135	132	0.98	0.08164	1.06	0.25219	3.89	0.0352	1.55	0.39751	285.1	79.7	228.4	8.0	222.9	3.4	0.10	98%
05	414	847	2.04	0.05028	2.04	0.25090	2.07	0.0352	1.50	0.72501	272.2	32.4	227.3	4.2	223.0	3.3	0.00	98%
06	86	78	0.91	0.09669	0.67	0.23194	5.26	0.0342	1.54	0.29268	157.7	113.6	211.8	10.1	216.7	3.3	0.15	98%
07	88	100	1.13	0.06948	0.94	0.23241	4.62	0.0347	1.54	0.33329	127.3	99.4	212.2	8.9	219.9	3.3	0.32	96%
08	101	117	1.16	0.10848	0.75	0.25217	3.22	0.0353	1.50	0.46647	274.0	63.9	228.3	6.6	223.9	3.3	0.13	98%
09	102	120	1.17	0.04979	1.54	0.23967	4.54	0.0347	1.53	0.33696	198.3	96.3	218.2	8.9	220.0	3.3	0.43	99%
10	132	153	1.16	0.05674	1.42	0.23841	3.68	0.0342	1.60	0.43510	220.4	74.9	217.1	7.2	216.8	3.4	0.27	100%
11	209	237	1.14	0.04912	2.98	0.23224	3.40	0.0332	1.51	0.44486	226.6	68.9	212.0	6.5	210.7	3.1	0.29	99%
12	175	230	1.32	0.04931	2.65	0.24209	3.11	0.0350	1.52	0.48759	204.0	61.8	220.1	6.2	221.6	3.3	0.12	99%
13	105	129	1.22	0.04969	2.24	0.24594	3.76	0.0346	1.53	0.40613	264.4	77.0	223.3	7.6	219.4	3.3	0.14	98%
14	157	213	1.36	0.09758	0.68	0.24102	2.85	0.0351	1.60	0.56204	185.3	54.0	219.3	5.6	222.4	3.5	0.13	99%
DSG07-3 (andesite)																		
01	951	197	0.21	0.04893	2.87	1.49135	1.62	0.1563	1.51	0.93234	905.0	12.1	926.9	9.9	936.1	13.2	0.02	99%
02	197	154	0.78	0.05039	2.19	3.81208	1.62	0.2805	1.51	0.93345	1597.1	10.8	1595.3	13.1	1594.0	21.4	0.01	100%
03	158	139	0.88	0.10848	0.79	0.28418	2.73	0.0407	1.51	0.55404	225.1	51.7	254.0	6.2	257.1	3.8	0.13	99%
04	239	103	0.43	0.05199	3.57	5.95896	3.21	0.3517	1.50	0.46750	1998.5	49.6	1969.9	28.3	1942.7	25.2	0.72	99%
05	895	311	0.35	0.05170	1.43	1.32042	1.83	0.1384	1.71	0.93328	904.7	13.5	854.7	10.7	835.6	13.4	0.03	98%
06	457	458	1.00	0.04921	5.03	0.23428	2.21	0.0339	1.50	0.68064	200.4	37.1	213.7	4.3	214.9	3.2	0.11	99%
07	194	91	0.47	0.04857	4.36	2.32432	1.85	0.2065	1.51	0.81794	1236.9	20.7	1219.7	13.2	1210.1	16.7	0.05	99%
08	482	216	0.45	0.05174	2.84	0.22862	2.54	0.0330	1.51	0.59454	208.1	46.6	209.1	4.8	209.1	3.1	0.16	100%
09	148	198	1.34	0.05007	4.27	3.68461	1.65	0.2764	1.50	0.91263	1561.2	12.6	1568.0	13.2	1573.1	21.0	0.04	100%
10	221	23	0.11	0.05055	3.31	1.38297	1.77	0.1444	1.50	0.84824	913.0	19.2	881.7	10.5	869.3	12.2	0.07	99%
11	103	97	0.95	0.05069	3.04	4.44010	1.68	0.2968	1.51	0.89615	1774.1	13.5	1719.9	14.0	1675.6	22.2	0.03	97%
12	543	1281	2.36	0.05019	2.71	0.24398	2.16	0.0355	1.51	0.69785	185.1	35.6	221.7	4.3	225.1	3.3	0.15	98%
13	208	104	0.50	0.05153	3.43	0.55844	2.07	0.0714	1.50	0.72656	481.5	31.1	450.5	7.6	444.5	6.5	0.00	99%
14	222	389	1.76	0.04979	2.36	0.23887	3.34	0.0353	1.50	0.45058	153.5	68.3	217.5	6.6	223.5	3.3	0.22	97%
15	196	254	1.30	0.06921	0.59	0.23633	3.05	0.0348	1.52	0.49640	162.6	60.8	215.4	5.9	220.3	3.3	0.17	98%
16	252	119	0.47	0.09856	0.58	0.27352	2.71	0.0399	1.53	0.56300	180.4	51.4	245.5	5.9	252.4	3.8	0.20	97%
17	185	109	0.59	0.05065	2.27	3.75853	1.65	0.2794	1.51	0.91238	1578.4	12.6	1583.9	13.3	1588.1	21.3	0.10	100%

f_{206} is the percentage of common ^{206}Pb in total ^{206}Pb.

Table 2
Laser ablation ICP-MS zircon U–Pb data of DSG07-5 and HN11-4 in the Southern Yidun.

spots	U	Th	Th/U	$^{207}Pb/^{206}Pb$		$^{207}Pb/^{235}U$		$^{206}Pb/^{238}U$		$^{207}Pb/^{206}Pb$		$^{207}Pb/^{235}U$		$^{206}Pb/^{238}U$		Concordance
	ppm	ppm		Ratio	±1σ	Ratio	±1σ	Ratio	±1σ	Age	±1σ	Age	±1σ	Age	±1σ	
DSG07-5 (trachyandesite)																
01	1172	854	1.37	0.0519	0.0032	0.2475	0.0149	0.0346	0.0004	280	106	225	12	219	3	97%
02	452	513	0.88	0.0513	0.0028	0.2425	0.0123	0.0345	0.0005	254	124	220	10	219	3	99%
03	279	753	0.37	0.1536	0.0028	10.1010	0.1851	0.4712	0.0043	2387	31	2444	17	2489	19	98%
04	817	596	1.37	0.0830	0.0041	1.1105	0.0486	0.0962	0.0017	1278	96	758	23	592	10	75%
05	245	356	0.69	0.1553	0.0032	10.7028	0.2238	0.4943	0.0055	2405	35	2498	19	2589	24	96%
06	552	625	0.88	0.0643	0.0031	0.3083	0.0148	0.0346	0.0005	754	99	273	12	219	3	78%
07	236	423	0.56	0.1606	0.0038	9.8619	0.2336	0.4419	0.0056	2462	40	2422	22	2359	25	97%
08	445	348	1.28	0.0621	0.0037	0.2976	0.0162	0.0362	0.0006	677	329	265	13	229	4	85%
09	132	3041	0.04	0.0535	0.0014	0.2656	0.0069	0.0357	0.0004	350	55	239	6	226	2	94%
10	556	607	0.92	0.0690	0.0032	0.3304	0.0160	0.0346	0.0005	898	105	290	12	219	3	72%
11	521	811	0.64	0.0734	0.0024	0.9463	0.0325	0.0926	0.0012	1033	60	676	17	571	7	83%
12	1392	1057	1.32	0.0527	0.0021	0.2382	0.0093	0.0329	0.0004	322	123	217	8	209	3	96%
13	71.8	178	0.40	0.0722	0.0047	1.3364	0.0902	0.1350	0.0033	992	133	862	39	816	19	94%
14	253	965	0.26	0.1633	0.0150	10.4525	0.9880	0.4613	0.0150	2490	154	2476	88	2445	66	98%
15	517	924	0.56	0.1722	0.0219	10.5122	1.3756	0.4407	0.0197	2579	214	2481	122	2354	88	94%
16	130	211	0.62	0.0983	0.0022	3.4018	0.0712	0.2520	0.0032	1591	42	1505	16	1449	16	96%
17	233	197	1.18	0.0863	0.0045	0.4789	0.0259	0.0400	0.0007	1346	100	397	18	253	4	55%
18	180	155	1.16	0.0728	0.0036	0.3591	0.0171	0.0361	0.0006	1009	100	312	13	228	4	69%
19	829	1155	0.72	0.0584	0.0017	0.2988	0.0103	0.0366	0.0005	546	65	265	8	232	3	86%
20	711	1071	0.66	0.0525	0.0014	0.2246	0.0058	0.0309	0.0003	309	55	206	5	196	2	95%
21	487	571	0.85	0.0539	0.0028	0.2482	0.0113	0.0337	0.0006	365	112	225	9	214	3	94%
22	338	1970	0.17	0.1140	0.0017	5.3357	0.0929	0.3382	0.0044	1865	32	1875	15	1878	21	99%
HN11-4 (trachyandesite)																
01	535	413	0.77	0.0542	0.0019	0.2562	0.0087	0.0341	0.0005	389	80	232	7	216	3	93%
02	162	168	1.04	0.0496	0.0028	0.2421	0.0119	0.0362	0.0006	176	131	220	10	229	4	96%
04	417	343	0.82	0.0496	0.0017	0.2421	0.0082	0.0352	0.0004	176	79	220	7	223	3	99%
05	122	114	0.93	0.0463	0.0026	0.2199	0.0115	0.0351	0.0006	13.06	125.9	202	10	222	4	91%
06	198	177	0.89	0.0491	0.0026	0.2241	0.0124	0.0333	0.0006	154	119	205	10	211	4	97%
07	306	280	0.91	0.0534	0.0020	0.2534	0.0090	0.0345	0.0004	346	85	229	7	219	3	95%
08	177	220	1.24	0.0626	0.0031	0.2856	0.0138	0.0334	0.0005	694	106	255	11	212	3	79%
09	301	348	1.16	0.0491	0.0018	0.2286	0.0083	0.0337	0.0004	154	87	209	7	214	2	98%
10	381	356	0.93	0.0453	0.0018	0.2113	0.0079	0.0338	0.0005			195	7	214	3	91%
11	206	196	0.95	0.0460	0.0023	0.2139	0.0101	0.0342	0.0006			197	8	217	4	91%
12	153	170	1.11	0.0489	0.0025	0.2277	0.0114	0.0343	0.0006	146	122	208	9	218	4	96%
13	123	144	1.17	0.0551	0.0030	0.2754	0.0137	0.0374	0.0007	417	156	247	11	236	4	96%
14	78.2	103	1.32	0.0591	0.0037	0.2662	0.0149	0.0341	0.0007	572	135	240	12	216	4	89%
15	206	223	1.08	0.0501	0.0022	0.2563	0.0108	0.0373	0.0006	211	104	232	9	236	4	98%
16	657	440	0.67	0.0544	0.0018	0.2641	0.0082	0.0352	0.0005	387	69	238	7	223	3	93%
17	317	319	1.01	0.0466	0.0020	0.2245	0.0092	0.0350	0.0005	31.6	100	206	8	222	3	93%
18	218	222	1.01	0.0467	0.0020	0.2393	0.0103	0.0371	0.0006	31.6	169	218	8	235	4	93%
20	265	250	0.94	0.0636	0.0026	0.3109	0.0135	0.0350	0.0006	728	87	275	10	222	3	76%
21	142	141	0.99	0.0516	0.0024	0.2509	0.0115	0.0357	0.0006	333	103	227	9	226	4	99%
22	798	531	0.67	0.0497	0.0015	0.2357	0.0070	0.0343	0.0003	189	70	215	6	218	2	99%
23	310	308	0.99	0.0523	0.0017	0.2425	0.0080	0.0337	0.0004	298	69	221	7	214	3	97%
24	279	227	0.81	0.0536	0.0023	0.2383	0.0093	0.0328	0.0005	354	101	217	8	208	3	96%

vary from 708 Ma to 848 Ma, with an average of 784 Ma (Table 3). The only negative $\varepsilon_{Hf}(t)$ value of −39.7 (Table 3) for spot 3 is believed to represent that of an inherited zircon grain. Scattered $\varepsilon_{Hf}(t)$ values and T_{DM1} model ages of 14 spot analyses for zircons from the sample DSG07-3 vary from −33.4 to 3.0 and from 718 Ma to 2222 Ma, respectively. 6 out of 14 analyses for zircon grains with oscillatory zoning in their CL images exhibit slightly negative to positive $\varepsilon_{Hf}(t)$ values from −1.3 to 3.7 and relatively young T_{DM1} model ages ranging from 718 Ma to 929 Ma. They are consistent with those of the sample DSG07-7. Other 8 analyses show much negative $\varepsilon_{Hf}(t)$ values ranging from −8.4 to −33.4 and much old T_{DM1} model ages varying from 1238 Ma to 2222 Ma. In summary, the magmatic zircons with $^{206}Pb/^{238}U$ ages of ca. 220 Ma have uniform initial Hf compositions with most $\varepsilon_{Hf}(t)$ values varying from 0 to 4.0 and the T_{DM1} model ages varying from 700 Ma to 900 Ma, while, the inherited zircons exhibit significantly negative $\varepsilon_{Hf}(t)$ values.

4.3. Mineral chemistry

Plagioclase is one of the major crystallizing phases for the most of the Southern Yidun volcanic rocks. In a trachyandesite sample (DSG11-34), the plagioclase phenocrysts contain 5.60–6.97 wt.% Na_2O, 7.37–10.15 wt.% CaO, and 0.25–0.83 wt.% K_2O. Their corresponding An values of 36–49 indicate that they are andesine (Appended Table 1). Clinopyroxene is a subordinate phenocryst and contains 54.26–56.99 wt.% SiO_2, 14.63–17.52 wt.% MgO, 9.55–13.39 wt.% $FeO_{(t)}$, and 12.05–15.09 wt.% CaO. They are typical augite with Mg# values varying from 66 to 76 and enstatite (En) percentages varying from 45 to 53 mol% (Appended Table 2). Amphibole is another dominant phase in the phenocrysts in the rocks. In a typical trachyandesite sample (XJP11-29), amphibole contains 41.23–44.82 wt.% SiO_2, 11.21–15.36 wt.% MgO, 11.65–17.53 wt.% $FeO_{(t)}$, 10.91–12.06 wt.% CaO, 9.62–11.18 wt.% Al_2O_3, 1.93–3.07 wt.% TiO_2, 1.88–2.25 wt.% Na_2O and 0.95–1.36 wt.% K_2O (Table 4). Using a 15eNK method for estimating the minimum proportion of total Fe as Fe^{3+}, the amphibole can be classified as calcium amphibole [$Ca_B \geq 1.5$, $(Na + K)_A \geq 0.50$, $Ti < 0.50$], and called pargasite (Leake et al., 1997).

4.4. Whole-rock geochemistry

Major and trace elemental compositions of the Late Triassic volcanic rocks from the Southern Yidun arc are shown in Table 5. Most

volcanic rocks are subjected to various degrees of alterations, as seen from the high LOI values ranging from 1.13 wt.% up to 8.00 wt.% (mostly between 2.00 wt.% and 4.00 wt.%). Their major oxide contents (recalculated to 100% in a volatile-free) vary widely, with SiO_2 contents ranging from 50.43% to 64.12%, Al_2O_3 from 13.67% to 19.52%, MgO from 1.24% to 6.85%, CaO from 1.24% to 9.71%, and $Fe_2O_{3(t)}$ from 4.90% to 12.41%, respectively. The relative high total alkali values ($Na_2O + K_2O$, 5.25–8.77%) and variations in K_2O/Na_2O ratio (0.25–2.53) could be a result of the hydrothermal alteration. Thus, the K_2O–SiO_2 and/or TAS diagrams conventionally used to classify igneous rocks are not suitable in our case. However, some high field strength elements (HFSEs; Zr, Hf, Nb, Ta, Ti, Y), Th and rare earth elements (REEs) apart from Eu and La are considered to be immobile during low-temperature alteration processes (e.g., Hastie et al., 2007; Pearce and Peate, 1995), the Zr/TiO_2 versus Nb/Y and Th versus Co diagrams are applied instead in this study. On the Zr/TiO_2 versus Nb/Y diagram (Pearce, 1996) (Fig. 6a), the analyzed samples are mainly plotted into trachyandesite areas, with minor samples plotted into alkali basalt area, well in accordance with the petrography of these rocks. On the Th versus Co diagram (Hastie et al., 2007) (Fig. 6b), all the samples are plotted into the field of high-K calc-alkaline and/or shoshonite series. In general, rock types classified in Fig. 6b are similar to those defined in Fig. 6a.

Although the trace element contents of the Zhongdian volcanic rocks are largely variable, their primitive mantle-normalized trace element patterns are mostly similar to each other (Fig. 7a), indicating that they could have shared a common parental magma or most likely were derived from a similar source with a similar petrogenesis (e.g., Mo et al., 2007). They are enriched in LILEs (such as Ba, Th, and Sr), and depleted in Nb, Ta and Ti, similar to that of "arc-type" lavas (Tatsumi et al., 1986). On the chondrite-normalized REE diagram, they are characterized by strong LREE enrichment, with $(La/Yb)_N$ values varying from 16.6 to 32.0, and no or weak Eu anomalies with Eu/Eu* ratios varying from 0.68 to 1.02 (Table 5, Fig. 7b).

The analyzed results of whole-rock Sr–Nd–Pb isotopes are given in Tables 6 and 7. The initial $^{87}Sr/^{86}Sr$ and $\varepsilon_{Nd}(t)$ values are calculated at the age of 220 Ma (zircon U–Pb ages). The studied volcanic rocks in

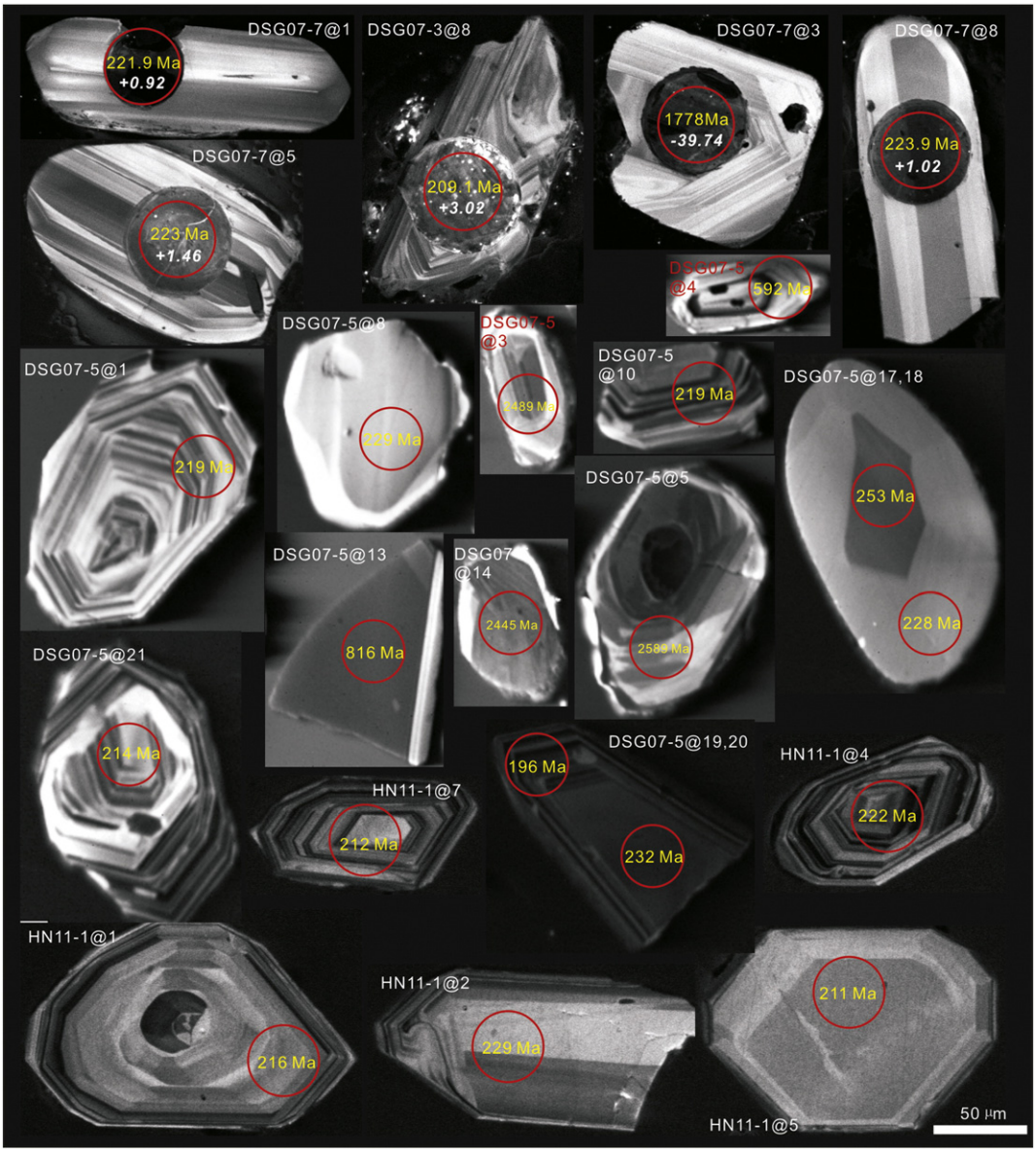

Fig. 4. Cathodoluminescence (CL) images of representative zircon grains from the Southern Yidun volcanic rocks. The red circles indicate the analyzed spots, and the yellow figures in these circles represent their $^{206}Pb/^{238}U$ ages, while the italic white figures represent their $\varepsilon_{Hf}(220\ Ma)$ values.

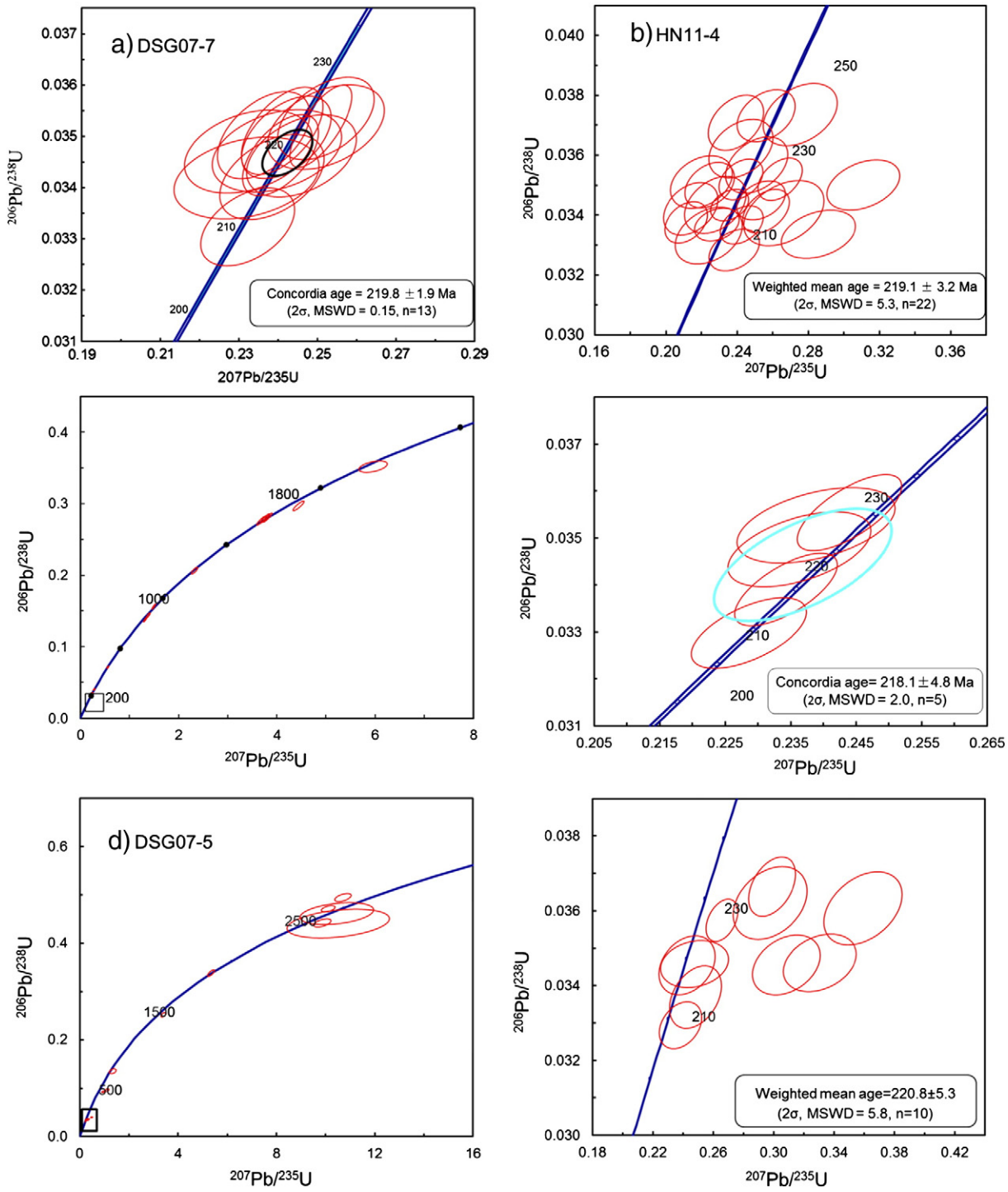

Fig. 5. Diagrams showing zircon U–Pb concordia ages for some volcanic rocks from the Zhongdian.

the Zhongdian region are characterized by relatively homogenous initial $^{87}Sr/^{86}Sr$ ratios from 0.7057 to 0.7060, and $\varepsilon_{Nd}(t)$ values varying from −2.7 to +0.7, with corresponding depleted-mantle Nd model ages (T_{DM}) ranging from 0.9 to 1.1 Ga. Their whole-rock Pb isotope compositions are very similar. They are characterized with a high radiogenic Pb isotopic composition, with present-day whole-rock $^{206}Pb/^{204}Pb$ $^{207}Pb/^{204}Pb$ and $^{208}Pb/^{204}Pb$ ratios varying from 18.078 to 18.369, from 15.570 to 15.619, and from 38.223 to 38.650, respectively. Their calculated initial ratios of $(^{206}Pb/^{204}Pb)_t$, $(^{207}Pb/^{204}Pb)_t$, and $(^{208}Pb/^{204}Pb)_t$ vary from 17.922 to 17.995, from 15.560 to 15.602, and from 37.904 to 38.086, respectively.

5. Discussions

5.1. The eruption timing of the Qugasi and Tumugou volcanic rocks from the Southern Yidun arc

The Yidun Arc is one of the largest island-arc among the Sanjiang Tethyan Orogenic Belt. It has long been proposed that the Yidun Arc was developed during the westward subduction of the Garzê–Litang Ocean in Late Triassic (Hou et al., 2003; Mo et al., 1993; Reid et al., 2007). Previous radiometric data for the syn-collisional granitoids in the Yidun arc indicate that the subduction of oceanic crust occurred

Table 3
Results of Hf isotope analysis on zircons of the DSG07-7 and DSG07-3 samples from the Southern Yidun.

Spots	t*(Ma)	$^{176}Yb/^{177}Hf$	±2σ	$^{176}Lu/^{177}Hf$	±2σ	$^{176}Hf/^{177}Hf$	±2σ	$\varepsilon_{Hf}(t)^{**}$	ε_{Hf}(220 Ma)	±2σ	T_{DM1}(Ma)	±2σ	T_{DM2}(Ma)
DSG07-7													
1	221.9	0.062438	0.001472	0.002036	0.000045	0.282670	0.000025		0.92	0.87	848	36	1194
2	219.5	0.049049	0.000770	0.001700	0.000026	0.282742	0.000028		3.52	0.97	737	40	1030
3	1778.3	0.027242	0.000448	0.000817	0.000010	0.281516	0.000022	−5.79	−39.74	0.79	2416	31	2803
4	222.9	0.029715	0.000467	0.001017	0.000017	0.282725	0.000021		3.02	0.73	747	29	1060
5	223.0	0.043410	0.001003	0.001454	0.000032	0.282683	0.000022		1.46	0.78	816	32	1160
6	216.7	0.022048	0.000214	0.000781	0.000007	0.282688	0.000017		1.75	0.59	794	23	1145
7	219.9	0.020481	0.000230	0.000686	0.000007	0.282703	0.000021		2.29	0.75	771	29	1109
8	223.9	0.035646	0.001770	0.001202	0.000057	0.282669	0.000020		1.02	0.72	830	29	1187
9	220.0	0.029189	0.000353	0.001031	0.000012	0.282672	0.000020		1.13	0.71	823	28	1182
10	216.8	0.042583	0.000632	0.001482	0.000021	0.282718	0.000023		2.72	0.82	766	33	1083
11	210.7	0.036432	0.000293	0.001295	0.000010	0.282757	0.000018		4.10	0.65	708	26	999
12	221.6	0.038555	0.001120	0.001416	0.000042	0.282704	0.000027		2.24	0.97	784	39	1111
DSG07-3													
1	936.1	0.067664	0.000525	0.002393	0.000020	0.282408	0.000029	6.35	−8.39	1.01	1238	42	1401
2	1594.0	0.073218	0.000442	0.002519	0.000013	0.282025	0.000027	6.37	−21.97	0.95	1799	39	1908
3	257.1	0.023842	0.000106	0.000823	0.000002	0.282691	0.000019	2.65	1.85	0.67	791	27	1114
4	1942.7	0.054606	0.001748	0.001753	0.000046	0.281697	0.000027	3.09	−33.44	0.96	2222	38	2381
5	835.6	0.041811	0.002969	0.001341	0.000097	0.282314	0.000018	1.52	−11.56	0.62	1336	25	1628
6	214.9	0.041290	0.000696	0.001550	0.000025	0.282605	0.000020		−1.30	0.71	929	29	1340
7	1210.1	0.042190	0.001523	0.001354	0.000040	0.281811	0.000019	−8.27	−29.36	0.67	2041	27	2525
8	209.1	0.025886	0.000165	0.000894	0.000006	0.282724	0.000018		3.02	0.63	745	25	1069
9	1573.1	0.038247	0.000525	0.001458	0.000018	0.281979	0.000026	5.42	−23.45	0.92	1812	36	1951
10	869.3	0.024947	0.001017	0.000853	0.000034	0.282319	0.000027	2.70	−11.32	0.94	1312	37	1580
12	225.1	0.026311	0.001215	0.000950	0.000044	0.282745	0.000021		3.73	0.75	718	30	1014
14	223.5	0.045043	0.000182	0.001609	0.000007	0.282674	0.000023		1.13	0.80	832	32	1180
15	220.3	0.035274	0.000479	0.001270	0.000015	0.282679	0.000021		1.36	0.74	818	30	1168
17	1588.1	0.026156	0.000618	0.001022	0.000018	0.282009	0.000021	7.29	−22.31	0.75	1749	29	1846

Note: t* denotes the $^{206}Pb/^{238}U$ age of zircon (Table 1); the ε_{Hf}(220 Ma) ratios were calculated at t = 220 Ma; the $\varepsilon_{Hf}(t)^{**}$ ratios were calculated at their determined $^{206}Pb/^{238}U$ age of zircon.

during the period from ca. 238 Ma to 210 Ma (Hou et al., 2004). Our SIMS and LA–ICP-MS zircon U–Pb dating results suggest that these volcanic rocks from the Southern Yidun arc (Zhongdian arc) erupted at ca. 220 Ma, well in accordance with the subduction timing of the Garzê–Litang Ocean (Hou et al., 2003). Thus, our dating results provide extra evidence that these Late Triassic volcanic rocks in the Southern Yidun are intimately associated with the subduction-related magmatism.

5.2. The evolving volcanic rocks: alteration and crystallization evaluation

As mentioned above, the volcanic rocks from the Qugasi and Tumugou Formations mainly include trachyandesites, and minor alkali basalts. Due to the intensely-altered character of the basaltic rocks and relative freshness of andesites, almost all of our samples came from the latter. However, alteration effects could still be detected both under the microscope and from the analyses of major element contents

Table 4
Representative electron microprobe analyses of amphibole in the trachyandesite (XJP11-29) from the Southern Yidun.

Spots	1	2	3	4	5	6	7	8	9	10	11	12	13	14	15
Na_2O	1.88	2.19	2.24	2.16	1.95	1.97	2.1	2.19	2.17	2.09	2.22	2.11	2.25	2.13	1.99
MgO	14.04	13.65	14.11	12.77	11.21	11.63	11.44	11.72	12.58	12.73	13.25	11.94	14.68	15.36	11.93
Al_2O_3	10.81	10.42	10.25	9.89	10.12	9.62	10.26	9.69	11.02	9.89	11.18	9.94	10.41	9.99	9.73
SiO_2	44.19	44.16	44.27	43.5	41.23	43.09	41.77	43.46	42.37	43.28	42.95	42.88	43.43	44.82	44.18
K_2O	1.05	1.09	1.06	1.09	1.36	1.19	1.23	1.13	1.18	1.07	1.15	1.22	1.1	0.95	1.28
CaO	11.66	11.97	11.8	11.72	11.69	11.54	11.63	11.75	11.68	10.91	11.92	11.79	12.06	11.14	11.52
TiO_2	2.36	2.43	2.38	2.07	2.33	2.12	2.35	2.1	2.56	1.94	3.07	2.28	2.6	2.43	1.93
MnO	0.2	0.24	0.25	0.32	0.37	0.43	0.41	0.4	0.28	0.31	0.26	0.39	0.14	0.24	0.43
FeO	13.13	13.55	12.33	15.54	17.53	17.23	17.25	16.46	14.55	15.03	12.83	16.71	12.08	11.65	16.74
Total	99.31	99.71	98.69	99.06	97.8	98.82	98.44	98.89	98.38	97.24	98.82	99.26	98.74	98.7	99.73
Mg#	0.67	0.64	0.67	0.61	0.58	0.57	0.57	0.56	0.61	0.6	0.65	0.58	0.7	0.7	0.56
Na	0.53	0.619	0.634	0.619	0.573	0.571	0.611	0.632	0.626	0.608	0.631	0.607	0.637	0.601	0.571
Mg	3.039	2.962	3.076	2.81	2.528	2.587	2.561	2.605	2.786	2.849	2.899	2.642	3.197	3.324	2.626
Al	1.851	1.789	1.766	1.722	1.805	1.692	1.815	1.703	1.93	1.75	1.935	1.739	1.792	1.71	1.693
Si	6.418	6.431	6.474	6.424	6.239	6.432	6.27	6.478	6.296	6.5	6.307	6.366	6.344	6.508	6.523
K	0.194	0.203	0.198	0.205	0.262	0.226	0.235	0.215	0.224	0.205	0.215	0.231	0.205	0.175	0.24
Ca	1.814	1.867	1.849	1.855	1.896	1.845	1.87	1.877	1.859	1.755	1.875	1.875	1.888	1.733	1.822
Ti	0.257	0.266	0.261	0.23	0.265	0.238	0.266	0.235	0.286	0.22	0.339	0.254	0.286	0.265	0.215
Mn	0.025	0.03	0.031	0.04	0.048	0.055	0.053	0.05	0.035	0.039	0.032	0.049	0.017	0.029	0.054
Fe^{3+}	0.074	0.000	0.000	0.145	0.351	0.171	0.268	0.024	0.056	0.000	0.000	0.184	0.105	0.000	0.021
Fe^{2+}	1.521	1.651	1.508	1.774	1.867	1.98	1.898	2.028	1.752	1.888	1.575	1.891	1.371	1.415	2.047
Total	15.723	15.818	15.798	15.824	15.835	15.797	15.846	15.847	15.85	15.813	15.809	15.838	15.842	15.76	15.811
P (kbar)	5.7	5.3	5.2	5.0	5.5	4.8	5.5	4.8	6.1	5.1	6.2	5.1	5.4	4.9	4.8
Depth (km)	20.7	19.4	18.9	18.1	20.0	17.5	20.1	17.6	22.3	18.6	22.4	18.5	19.5	17.8	17.4

Note: Mg# = 100 × Mg / (Mg + Fe) in atomic ratio; the proportion of Fe^{3+} is corrected using a 15eNK method for the minimum estimate (Leake et al., 1997); pressure calculation equation: P (kbar) = 5.64 × Al^{total} − 4.76 (Hollister et al., 1987).

Table 5
Major oxides and trace element concentrations of the Late Triassic volcanic rocks from the Southern Yidun.

Sample	Tumugou Formation																Tumugou Formation					
	DSG04-1	DSG04-2	DSG04-3	DSG07-1	DSG07-3-1	DSG07-3-2	DSG07-4	DSG07-5	DSG07-7	DSG07-8	DSG07-8-2	DSG10-1	DSG11-2	DSG10-3	DSG10-4	DSG10-5	DSG10-6	DSG10-7	DSG10-8	DSG10-11	DSG10-12	DSG10-13
Major oxides (wt.%)																						
SiO_2	55.18	51.59	52.61	59.77	57.59	58.30	53.62	54.11	55.13	62.14	60.98	54.89	50.75	58.00	57.25	55.16	58.26	57.43	55.92	56.88	52.73	57.55
Al_2O_3	15.15	15.77	15.80	14.99	13.26	15.64	15.30	17.19	13.89	14.26	14.26	15.78	21.92	15.65	16.79	15.42	16.48	16.07	15.64	14.89	16.71	15.82
$Fe_2O_{3(t)}$	8.76	9.84	9.39	6.77	7.96	6.01	8.94	8.07	8.71	5.89	5.90	5.71	8.07	5.49	4.85	5.69	4.92	6.55	5.74	6.73	8.69	5.86
CaO	6.03	7.30	6.27	6.96	6.38	9.55	7.70	4.02	5.32	3.96	4.34	5.67	1.73	4.55	3.66	5.07	4.52	4.27	5.48	4.61	6.87	7.33
MgO	4.90	5.41	5.27	2.54	4.80	1.83	4.98	4.34	4.42	1.62	1.67	2.53	2.46	1.97	1.82	3.00	1.17	1.28	2.28	3.70	4.37	2.09
Na_2O	3.18	2.59	2.99	4.66	2.92	4.32	3.16	3.18	2.12	4.65	4.70	3.74	3.24	4.21	4.65	4.43	4.95	5.49	4.30	2.50	4.15	4.12
K_2O	1.99	2.16	2.26	1.53	2.64	1.33	1.95	4.87	5.37	3.35	3.38	2.24	4.63	2.54	2.55	1.57	2.44	1.38	2.82	2.71	1.46	2.22
MnO	0.13	0.15	0.14	0.12	0.13	0.13	0.14	0.11	0.13	0.10	0.11	0.10	0.07	0.09	0.06	0.10	0.05	0.05	0.09	0.10	0.13	0.08
P_2O_5	0.42	0.42	0.44	0.36	0.31	0.33	0.37	0.48	0.35	0.33	0.32	0.40	0.24	0.39	0.42	0.40	0.43	0.43	0.37	0.33	0.38	0.33
TiO_2	1.45	1.53	1.50	1.15	1.04	0.92	1.18	1.16	1.07	0.93	0.93	0.72	1.02	0.74	0.80	0.74	0.76	0.74	0.70	1.08	1.31	0.99
LOI	2.02	2.38	2.51	1.13	1.47	1.63	2.61	2.30	3.42	2.39	2.80	7.03	4.29	5.69	5.22	6.65	4.59	4.24	5.28	5.11	1.99	1.20
Total	99.20	99.14	99.19	99.98	98.49	99.97	99.96	99.83	99.93	99.61	99.38	98.81	98.42	99.32	98.07	98.23	98.57	97.93	98.62	98.64	98.79	97.59
Mg#	53	52	53	43	54	38	52	52	50	35	36	47	38	42	43	51	32	28	44	52	50	41
Trace elements (ppm)																						
Cs	1.90	3.50	2.43	1.83	3.56	1.11	3.27	2.90	7.75	4.51	4.72	2.61	7.07	2.79	2.59	2.07	2.06	1.11	4.20	3.92	2.73	1.43
Rb	55.3	80.2	71.5	31.5	70.3	23.1	55.0	101	140	88.8	90.7	58.3	131	56.1	65.1	40.6	67.2	35.3	75.3	59.2	58.6	47.1
Ba	1447	1298	1710	1307	5233	1449	1518	11526	13007	4984	5146	2010	4110	2910	2460	1725	2060	976	1780	4130	1020	2470
Th	14.2	15.8	15.6	11.9	10.0	12.9	11.5	14.5	10.8	15.5	15.4	19.5	27.5	18.9	21.1	19.2	21.2	20.1	19.4	12.9	14.9	15.1
U	2.63	2.91	2.90	2.80	2.43	2.98	2.82	3.71	4.88	3.06	3.14	3.32	1.15	3.94	4.50	3.96	4.57	3.57	4.08	3.06	3.00	3.24
Ta	1.44	1.61	1.59	0.88	0.83	0.88	0.94	1.17	0.89	1.10	1.09	1.00	1.40	1.00	1.10	1.00	1.10	1.10	1.10	0.90	1.20	0.90
Nb	16.6	18.4	18.0	13.7	11.9	12.3	13.6	17.8	12.7	15.7	14.8	14.2	19.8	14.1	15.9	14.2	15.3	14.8	13.9	12.7	16.5	13.4
Sr	1100	1411	1163	1470	1190	1890	1629	1120	987	1090	1090	1650	1475	2080	1710	1825	1845	1510	1265	1190	1570	2010
Zr	173	191	188	176	150	170	171	215	156	201	198	178	259	175	196	179	187	181	182	165	213	176
Hf	4.98	5.44	5.40	4.18	3.90	4.41	4.40	5.28	4.33	5.04	4.90	4.60	6.60	4.60	5.20	4.60	5.10	4.70	4.60	4.30	5.40	4.60
Y	22.4	23.7	22.6	18.7	17.4	16.1	18.4	20.8	17.4	15.8	15.8	16.2	23.9	17.3	16.6	15.8	16.9	19.7	17.0	18.3	21.6	17.6
Pb	32.7	42.2	33.1	30.3	32.6	45.5	37.1	29.0	28.2	19.5	19.6	17.0	7.00	13.0	11.0	54.0	19.0	10.0	21.0	28.0	40.0	38.0
V	186	201	201	225	226	269	251	224	224	143	140	161	179	161	182	170	164	114	153	263	294	268
Cr	43.2	45.2	42.5	50.8	83.8	42.1	57.7	40.9	64.9	42.6	47.4	60.0	60.0	50.0	60.0	60.0	50.0	50.0	40.0	50.0	40.0	60.0
Co	22.3	25.7	25.0	12.9	26.8	7.2	29.0	21.0	26.0	13.2	13.0	16.3	14.6	23.3	12.9	19.0	15.6	12.2	14.8	19.0	25.5	11.8
Ni	25.8	27.6	26.7	22.4	36.2	15.8	33.3	22.4	33.1	17.5	31.8	21.0	24.0	33.0	22.0	27.0	17.0	18.0	24.0	19.0	24.0	18.0
La	49.2	55.7	51.2	44.5	37.4	44.2	39.7	54.5	40.7	48.7	48.4	61.1	75.5	61.9	67.0	60.5	66.0	60.1	54.8	46.5	55.1	55.0
Ce	91.3	97.5	93.9	80.0	68.9	77.8	75.5	98.8	74.7	84.8	84.2	108	139	110	122	108	118	112	103	85.5	106	97.4
Pr	10.7	12.1	11.6	9.10	7.96	8.68	8.84	11.1	8.72	9.28	9.25	11.6	16.1	11.9	12.9	11.5	12.5	12.6	11.5	9.72	12.0	10.8
Nd	41.3	45.8	44.2	33.1	30.6	31.9	33.0	40.3	32.8	34.1	33.1	40.8	56.9	40.9	44.9	40.2	43.7	44.7	40.6	35.3	44.7	38.3
Sm	7.57	8.22	8.08	5.79	5.71	5.40	5.85	7.09	5.87	5.76	5.75	6.58	9.28	6.87	7.35	6.59	7.01	7.13	6.58	6.37	8.01	6.55
Eu	2.01	2.24	2.11	1.70	1.57	1.59	1.83	1.59	1.36	1.44	1.42	1.62	2.2	1.64	1.65	1.36	1.79	1.72	1.61	1.66	2.09	1.73
Gd	6.45	7.01	6.79	4.80	4.92	4.58	5.10	5.80	5.56	4.60	4.79	5.83	8.15	6.01	6.28	5.66	6.16	6.40	5.72	5.67	6.95	5.71
Tb	0.84	0.91	0.86	0.67	0.69	0.62	0.72	0.81	0.70	0.65	0.66	0.67	0.98	0.72	0.74	0.66	0.73	0.77	0.69	0.72	0.90	0.71
Dy	4.62	4.99	4.81	3.65	3.66	3.41	3.90	4.22	3.72	3.48	3.34	3.28	4.58	3.40	3.47	3.18	3.49	3.78	3.34	3.63	4.57	3.51
Ho	0.85	0.93	0.90	0.72	0.69	0.65	0.76	0.81	0.70	0.63	0.62	0.59	0.86	0.64	0.65	0.59	0.63	0.71	0.63	0.69	0.85	0.66
Er	2.38	2.58	2.48	1.83	1.92	1.71	1.96	2.20	1.92	1.64	1.70	1.75	2.39	1.80	1.80	1.68	1.79	2.12	1.86	1.89	2.34	1.83
Tm	0.32	0.34	0.32	0.25	0.25	0.22	0.25	0.29	0.26	0.21	0.22	0.23	0.32	0.24	0.25	0.23	0.24	0.28	0.24	0.25	0.32	0.24
Yb	1.97	2.15	2.07	1.63	1.57	1.50	1.68	1.89	1.76	1.44	1.48	1.39	1.95	1.52	1.50	1.40	1.49	1.76	1.56	1.50	1.93	1.52
Lu	0.29	0.31	0.30	0.22	0.23	0.21	0.27	0.28	0.24	0.21	0.21	0.19	0.28	0.23	0.22	0.21	0.22	0.27	0.25	0.23	0.28	0.23
Eu/Eu*	0.87	0.90	0.86	0.98	0.90	0.97	1.02	0.75	0.72	0.85	0.82	0.79	0.77	0.78	0.74	0.68	0.83	0.77	0.80	0.84	0.85	0.86
$(La/Yb)_N$	17	17	17	18	16	20	16	19	16	23	22	30	26	27	30	29	30	23	24	21	19	24
Sr/Y	49	59	51	79	69	118	89	54	57	69	69	102	66	120	103	116	109	77	74	65	73	114

Note: Mg# = 100 × molar Mg / (Mg + Fe), the chondrite normalization values from Boynton, 1984.

Sample	Tumugou Formation									Tumugou Formation									Qugasi Formation					
	DSG10-15	DSG11-27	DSG11-29	DSG11-30	DSG11-31	DSG11-35	DSG11-36	LNT10-1	LNT10-2	LNT10-3	LNT10-4	X07-19	X07-20	XJP06-33	XJP06-34	XJP11-29	XJP11-30	XJP11-31	HN11-1	HN11-2	HN11-5	HN11-6	HN11-7	HN11-8
Major oxides (wt.%)																								
SiO_2	48.00	59.38	59.77	59.17	61.00	56.12	59.12	48.85	50.65	54.57	51.00	54.98	60.47	56.42	57.55	56.19	54.64	56.80	57.29	56.18	57.75	59.09	56.22	57.59
b,xAl_2O_3	17.28	14.70	14.83	14.83	14.90	15.62	15.58	16.92	18.49	16.60	14.50	14.28	14.92	13.48	13.11	15.41	14.80	15.53	15.62	15.12	15.24	14.98	15.28	15.64
$Fe_2O_{3(t)}$	10.14	4.95	4.72	4.59	4.86	5.58	5.82	11.71	10.62	6.41	7.66	7.68	7.16	6.75	7.39	7.23	6.91	6.82	6.11	6.12	5.90	5.54	5.86	6.14
CaO	3.80	4.05	3.73	3.72	3.82	5.32	3.68	2.14	1.89	6.01	6.36	4.74	1.20	5.39	5.34	3.76	5.22	2.79	3.98	4.66	3.74	3.55	4.47	3.44
MgO	6.30	2.89	2.94	3.43	2.63	2.25	1.41	6.47	5.58	2.89	4.18	4.72	3.24	2.80	2.55	4.06	4.13	4.15	2.59	2.94	2.88	2.62	2.69	2.86
Na_2O	3.74	3.67	3.93	3.81	3.28	3.93	3.61	3.48	3.83	4.61	2.17	2.47	3.30	2.08	2.10	4.13	3.55	3.95	4.48	4.08	5.32	5.03	3.73	4.70
K_2O	3.42	3.06	2.79	3.03	3.62	3.25	3.99	2.86	1.71	1.97	2.68	3.66	4.48	4.77	4.12	2.89	1.47	2.74	2.93	2.85	3.05	3.20	3.35	3.30
MnO	0.13	0.11	0.10	0.12	0.09	0.08	0.03	0.19	0.08	0.11	0.12	0.12	0.10	0.11	0.11	0.13	0.10	0.12	0.08	0.08	0.10	0.10	0.09	0.08
P_2O_5	0.47	0.31	0.32	0.31	0.34	0.37	0.36	0.36	0.33	0.27	0.28	0.66	0.72	0.65	0.63	0.42	0.40	0.43	0.46	0.45	0.43	0.39	0.44	0.45
TiO_2	1.91	0.58	0.61	0.60	0.59	0.67	0.69	1.41	1.53	1.35	1.11	1.32	1.39	1.28	1.26	1.26	1.25	1.29	1.12	1.18	1.06	0.98	1.07	1.09
LOI	2.79	4.45	4.71	4.95	4.47	5.20	4.01	3.72	5.04	3.78	8.00	5.86	2.85	5.77	5.36	2.68	5.78	3.51	3.75	5.04	3.13	3.07	4.96	2.69
Total	97.98	98.15	98.45	98.56	99.60	98.39	98.30	98.11	99.75	98.57	98.06	100.48	99.83	99.49	99.52	98.16	98.25	98.13	98.41	98.70	98.60	98.55	98.16	97.98
Mg#	55	54	55	60	52	44	32	52	51	47	52	55	47	45	41	53	54	55	46	49	49	48	48	48
Trace elements (ppm)																								
Cs	3.15	1.63	1.81	2.29	3.42	4.43	6.19	3.25	6.68	7.51	10.35	2.69	2.09	3.87	3.54	1.27	3.34	1.54	4.18	8.06	8.20	6.11	4.04	3.16
Rb	89.8	54.5	53.9	52.2	67.8	87.3	106.5	58.9	50.2	52.6	80.7	84.8	106.1	122.8	108.6	63.8	60.6	61.8	78.1	92.4	98.7	104.3	94.7	98.5
Ba	3730	3149	2179	2086	2198	2331	3257	3330	905	1400	1500	5128	6434	3143	2536	2574	1381	2455	2028	1992	1699	2109	2426	2317
Th	15.3	19.7	19.2	18.8	13.9	18.2	19.0	17.2	17.4	15.5	13.8	15.1	15.5	17.9	17.5	13.5	13.0	14.0	14.2	13.9	14.7	14.9	14.2	14.7
U	6.25	3.59	2.82	3.63	2.64	3.89	3.99	3.52	3.00	3.34	2.41	4.01	3.83	3.75	3.72	3.30	3.14	3.17	3.77	3.67	3.75	3.64	3.56	3.63
Ta	1.50	1.25	1.22	1.20	1.00	1.17	1.21	1.50	1.80	1.60	1.20	1.10	1.19	1.29	1.23	1.29	1.20	1.28	1.57	1.66	1.63	1.58	1.65	1.69
Nb	21.5	16.8	16.8	16.1	11.9	16.5	17.1	18.6	21.7	19.5	14.9	16.4	17.5	15.3	14.8	18.0	17.2	18.3	21.9	23.8	22.8	21.6	22.5	23.6
Sr	1020	691	794	792	607	1329	1418	651	286	1460	392	1147	652	1564	1043	1272	1211	1112	1211	1578	1084	1135	1238	1261
Zr	259	141	154	142	130	155	164	198	231	217	167	182	194	161	156	176	156	168	206	212	202	204	208	210
Hf	6.50	4.03	4.28	3.97	3.61	4.26	4.49	5.10	6.00	5.50	4.20	4.91	4.85	4.65	4.46	4.68	4.11	4.61	5.59	5.26	5.26	5.43	5.47	5.57
Y	28.1	13.9	12.8	13.6	14.7	15.8	17.2	22.1	21.0	20.8	18.0	17.5	18.3	17.8	17.2	16.2	16.3	16.8	19.3	19.5	19.3	18.0	19.1	19.6
Pb	26.0	10.9	16.9	10.3	13.8	51.4	54.9	16.0	25.0	34.0	15.0	20.7	27.6	28.7	27.8	13.5	18.2	45.5	32.3	20.8	43.9	21.3	14.7	20.4
V	299	117	123	120	115	142	142	249	222	197	193	230	217	152	154	192	188	198	150	150	141	134	141	150
Cr	40.0	14.9	20.2	24.4	18.3	29.4	52.4	20.0	20.0	20.0	20.0	43.2	62.9	210.0	252.8	30.2	27.0	30.9	10.6	29.8	10.8	10.1	9.1	10.2
Co	32.7	32.3	28.1	27.3	28.0	18.5	17.4	36.8	32.0	18.3	23.3	19.8	20.7	20.5	19.8	31.8	23.7	30.4	28.2	25.7	34.2	29.0	21.8	36.5
Ni	27.0	9.8	8.3	9.2	9.7	15.1	13.7	36.0	32.0	22.0	22.0	28.7	34.2	150.7	178.2	19.6	17.3	19.9	10.3	13.9	10.0	9.9	9.8	10.8
La	56.7	51.2	49.6	51.1	36.2	57.3	64.9	53.9	57.4	50.4	42.3	47.8	48.9	47.3	46.0	46.4	46.1	50.2	51.4	51.6	53.4	51.2	51.5	53.2
Ce	112	83.9	82.8	85.0	61.6	96.9	110.0	99.0	107.5	94.8	81.8	85.4	88.5	86.7	82.6	80.6	78.1	81.5	87.4	88.4	91.2	84.9	87.8	90.3
Pr	13.3	9.59	9.48	9.52	7.15	11.2	12.6	11.5	12.1	10.5	8.83	9.97	10.0	10.0	9.70	9.23	9.09	9.68	10.1	10.4	10.6	10.1	10.0	10.6
Nd	49.9	32.8	32.5	33.0	26.4	38.3	43.6	41.7	43.0	37.4	31.9	37.7	37.8	38.7	37.4	34.0	33.3	35.1	36.6	37.4	38.2	35.6	36.3	38.1
Sm	9.55	5.25	5.11	5.38	4.70	5.95	7.24	7.23	7.22	6.49	5.63	7.08	7.04	7.06	6.84	5.98	5.96	6.29	6.19	6.56	6.61	6.00	6.12	6.66
Eu	2.26	1.53	1.42	1.51	1.46	1.66	2.01	1.93	2.08	1.92	1.55	1.82	1.63	1.84	1.83	1.86	1.85	1.99	1.96	1.99	1.90	1.75	1.90	1.92
Gd	8.48	5.30	4.78	4.93	4.55	5.68	6.71	6.68	6.64	6.11	5.34	5.68	5.61	6.02	5.63	5.81	5.56	6.05	5.92	6.19	6.20	5.73	5.97	6.57
Tb	1.14	0.61	0.58	0.60	0.59	0.69	0.79	0.87	0.85	0.81	0.70	0.77	0.77	0.73	0.69	0.72	0.74	0.77	0.79	0.81	0.83	0.76	0.79	0.82
Dy	5.86	2.75	2.48	2.68	2.78	3.03	3.51	4.34	4.35	4.31	3.65	4.13	4.07	3.86	3.70	3.38	3.42	3.47	3.73	3.91	3.80	3.59	3.78	3.91
Ho	1.07	0.56	0.52	0.53	0.61	0.60	0.73	0.84	0.84	0.80	0.68	0.78	0.74	0.70	0.66	0.68	0.67	0.69	0.79	0.78	0.77	0.73	0.80	0.80
Er	2.87	1.52	1.42	1.44	1.58	1.72	1.97	2.46	2.45	2.33	1.98	1.93	1.86	1.90	1.80	1.78	1.76	1.86	2.06	2.03	2.00	1.94	2.01	2.09
Tm	0.41	0.20	0.19	0.20	0.22	0.23	0.25	0.32	0.34	0.32	0.26	0.27	0.26	0.25	0.24	0.24	0.23	0.25	0.28	0.27	0.29	0.26	0.27	0.28
Yb	2.38	1.38	1.36	1.35	1.51	1.50	1.72	2.06	1.98	1.92	1.64	1.65	1.62	1.55	1.50	1.50	1.49	1.63	1.80	1.76	1.73	1.61	1.73	1.77
Lu	0.35	0.21	0.20	0.19	0.22	0.22	0.25	0.31	0.30	0.29	0.25	0.24	0.24	0.24	0.22	0.22	0.21	0.22	0.26	0.25	0.23	0.23	0.25	0.24
Eu/Eu^*	0.76	0.88	0.87	0.89	0.96	0.87	0.88	0.84	0.91	0.93	0.86	0.87	0.79	0.86	0.89	0.96	0.97	0.98	0.98	0.95	0.90	0.91	0.95	0.88
$(La/Yb)_N$	16	25	25	25	16	26	25	18	20	18	17	20	20	21	21	21	21	21	19	20	21	21	20	20
Sr/Y	36	50	62	58	41	84	83	29	14	70	22	66	36	88	61	78	74	66	63	81	56	63	65	65

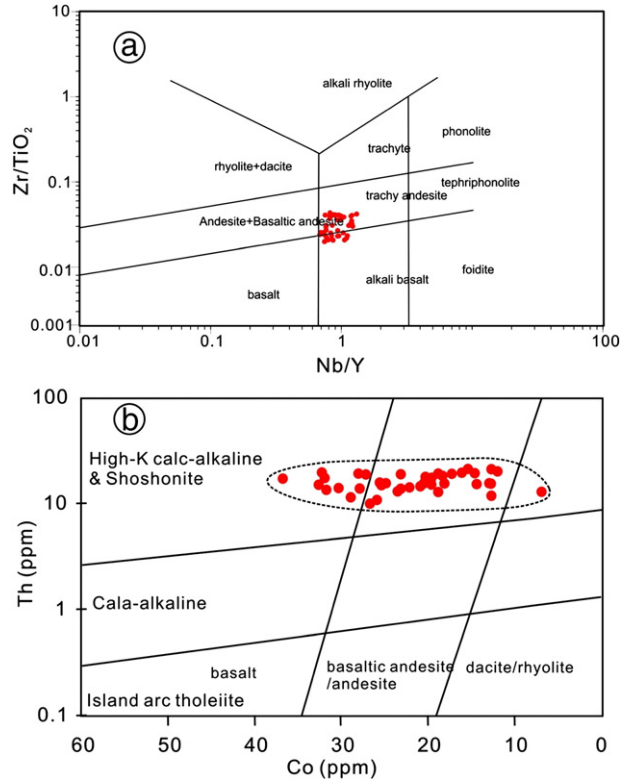

Fig. 6. Chemical compositions of the Southern Yidun volcanic rocks are plotted in (a) the Nb/Y vs. Zr/TiO_2 classification diagram (after Pearce, 1996) and (b) the Th vs. Co diagram (after Hastie et al., 2007).

of our samples, and they are represented by slight chloritic or propylitic alteration of primary minerals such as clinopyroxene, hornblende and plagioclase, and ambiguous distribution of Na_2O and K_2O contents (Fig. 8g, h), and to a lesser degree CaO and Al_2O_3 contents, with variations of SiO_2 in the Harker diagram (Fig. 8d, e), respectively. As a result, it is impossible to determine the lithology by using the TAS diagram ($Na_2O + K_2O$ vs. SiO_2). However, the revised Nb/Y vs. Zr/TiO_2 diagram by Pearce (1996) is widely used for classifying the altered volcanic rocks (Hastie et al., 2007), and our plotting results show that the bulk of our samples are trachyandesite with minor samples plotted into the area of alkali basalt, well in accordance with the field and microscopic observations.

Linear to semi-linear trends could still be seen from the variation of $Fe_2O_{3(t)}$ — MgO–TiO_2–MnO contents with SiO_2 contents (Fig. 8 a, b, c, f), though alteration did alter these compositions to a slight degree. These variations imply that they are controlled by fractional crystallization of one or two liquidus minerals, including clinopyroxene, hornblende, and Fe–Ti oxides; while the ambiguities shown by the Al_2O_3–CaO contents with SiO_2 variations imply either co-crystallization of three liquidus minerals including clinopyroxene, hornblende and plagioclase or variation of liquidus assemblage with proceeding crystallization, i.e., transition from clinopyroxene + plagioclase to hornblende +plagioclase (Fig. 8e), since both aluminum and calcium are major components in these three kinds of minerals.

According to Rollinson (1993), yttrium (Y) is incompatible to all the crystallizing phases in an intermediate to acid magmatic system, except hornblende, which has a Y partition coefficient of 2.5. In a series of typical arc lavas, the Y concentrations increase with increasing SiO_2 contents (e.g., Rohrlach and Loucks, 2005). However, the reverse trend shown by our samples in this study strongly suggests that hornblende is an important liquidus mineral in the crystallization sequence (Fig. 8i). Moreover, hornblende serves as a good geobarometer (Hollister et al., 1987), allowing us to give a proper estimate on the crystallization pressure and thus crystallization depth of this mineral. The calculated pressures for hornblende crystallization range from ~4.8 to 6.2 kbar, corresponding to a crystallization depth varying from 17 to 22 km.

Strontium (Sr) concentration in the magma is mostly controlled by the behavior of plagioclase in this case, since plagioclase has a Sr partition coefficient of 1.6 to 2.8 (Rollinson, 1993). The relatively constant Sr concentrations with variations in SiO_2 content suggest that plagioclase crystallization was suppressed while hornblende crystallized in comparison with normal arc andesites (Fig. 8j).

The crystallization of hornblende and suppressed crystallization of plagioclase give rise to high Sr/Y ratios of some samples that are one of the distinguishing features of adakites, and an obvious question would be: are the volcanic rocks in the Southern Yidun arc of adakitic affinity in origin or not?

5.3. Nature of the magma source and the petrogenesis of volcanic rocks from Southern Yidun arc

Subducting oceanic crust slab-melting is proposed in the early works of adakite petrogenesis (Defant and Drummond, 1990; Drummond and Defant, 1990). Moreover, further studies show that two distinct compositional groups of adakites, including high-SiO_2 Adakites (HSA) and low-SiO_2 Adakites (LSA), have been identified by examination of an extensive adakite geochemical database (e.g., Martin et al., 2005). The major difference in the petrogenesis of these two groups of adakites lies in the "effective melt/rock ratio" (i.e. subducting oceanic crust slab-melt/peridotite ratio; Rapp et al., 1999; Martin et al., 2005), with the HSA formed as a result of high melt/rock ratio and the LSA from a parental magma of low melt/rock ratio (Martin et al., 2005).

Thus it is of vital importance to determine contributions from different components within the arc system, including the subducting pelagic sediments, subducting oceanic crust (slab), lithospheric mantle wedge, and also continental crust, in terms of both fluids, melts and contamination, in the magma source, before we could draw a conclusion on the nature of the volcanic rocks from Southern Yidun arc.

Thorium (Th) is an incompatible element during the partial melting of no matter subducting sediments or slabs (e.g., Hawkesworth et al., 1997), and it is also an immobile element compared to Cerium (Ce) and Sr during fluid activities (e.g., Ayers, 1998; Ben Othman et al., 1989). Thus fluids derived from dehydration of subducting pelagic sediments are expected to have a low Th/Ce ratio but a high Sr/Th ratio; while partial melts from the subducting sediments would have a higher Th/Ce ratio with a lower Sr/Th ratio. As shown in the Th/Ce vs. Sr/Th diagram (Fig. 9), all the volcanic rocks from the Southern Yidun arc are plotted very close to the pelagic sediments (GLOSS), implying that partial melts rather than fluids from the subducting sediments are important contributors to the parental magma. Moreover, the steep trend on the plot of $^{206}Pb/^{204}Pb$ vs. $^{207}Pb/^{204}Pb$ and the shift towards the composition of EMII (Fig. 10) also suggest a component of recycled continent-derived materials involved into the source region.

HREE, Y, and Sr contents are the defining geochemical characteristics of adakites, and there are two widely-accepted discrimination diagrams: $(La/Yb)_N$ vs. Yb_N and Sr/Y vs. Y (Martin et al., 2005, and references therein). Since the Sr/Y ratio has largely been affected by the crystallization of hornblende, the plotting results from the latter diagram could not be trusted. In the $(La/Yb)_N$ vs. Yb_N diagram (Fig. 11), more than half of our samples are plotted into the adakite domain. Moreover, hornblende has relatively high Rare Earth Element (REE) levels in it, and it is especially enriched in Middle Rare Earth Elements (MREEs). As a consequence, relatively large amounts of hornblende crystallization from the parental magma would lead to a spoon-shaped REE pattern reflecting hornblende involvement in the fractionation schemes, however, this is not the case of the volcanic rocks from the Southern Yidun arc. Instead, they coincidently show a steeply right-declined REE pattern, with almost no or only slight Eu negative anomaly (Fig. 7b), implying that this REE pattern is probably dominated by the

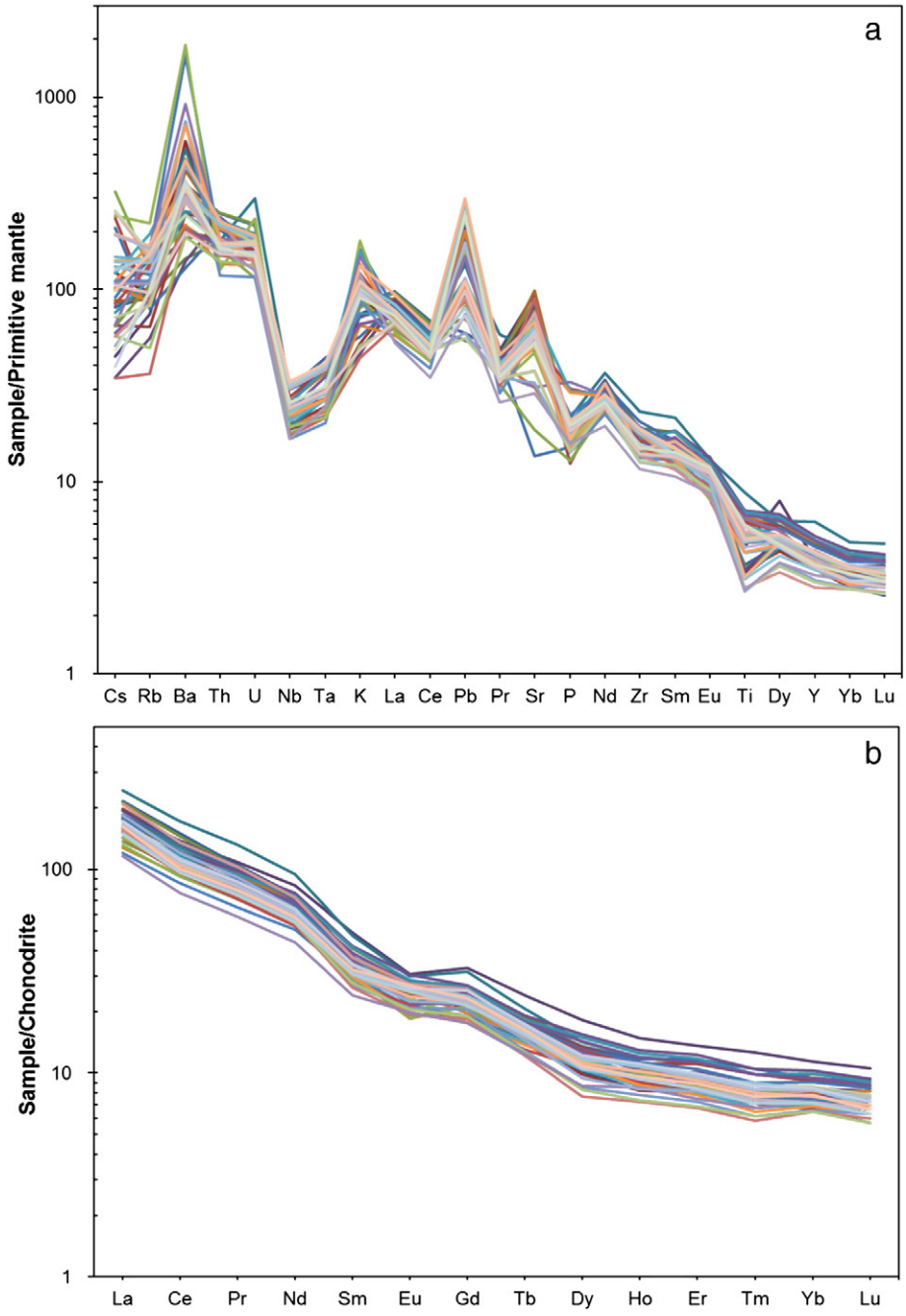

Fig. 7. Primitive mantle-normalized incompatible trace-element variation diagram (a) and chondrite-normalized rare earth element diagram (b) for the Southern Yidun volcanic rocks (primitive mantle values are from Sun and McDonough, 1989, and chondrite data are from Boynton, 1984, respectively).

residual garnet in the primary magma, rather than simply controlled by hornblende crystallization. According to reviews of Martin et al. (2005) and references therein, both HSA and LSA originated from magma sources with residual garnet, and the average Yb content of LSA is 0.93 ppm whereas it is 4.4 ppm in typical arc dacite. The volcanic rocks from the Southern Yidun arc contain Yb concentrations from 1.35 to 2.38 ppm with an average value of 1.67 ppm (Table 5), which is higher than that of LSA but lower than that of typical arc dacites, implying that both slab melts and melts from mantle peridotite are involved in the primary magma, with a probably low slab-melt/peridotite ratio, thus indicating that these rocks are of adakitic affinity in origin.

In the Sr–Nd isotope diagram (Fig. 12c), all samples are plotted in a very limited area, near to the mantle array, and at the same time show enriched characters. Moreover, both Sr and Nd isotopes show no considerable variation with SiO_2 contents (Fig. 12a, b), which allows us to preclude considerable contamination from the upper crust during magma ascending. These enriched characters could be brought about by the involvement of melts from the subducting sediments in the magma source; however, chances are that contamination from the lower crust also made a difference. There are several reasons for this. Firstly, a crystallizing depth varying from 17 to 22 km, obtained from the hornblende geobarometer, indicates a lower crust environment, implying that the magma may have been stagnated there in a magma chamber during which time interval hornblende crystallized. Secondly, all the zircon grains (11 out of 12 grains from DSG07-7 and 5 out of 17 grains from DSG07-3) giving concordant ages of ca. 220 Ma have positive ε_{Hf}(220 Ma) values ranging from 0.9 to 4.1 with an average value

Table 6
Data of whole-rock Sr and Nd isotopes for the Late Triassic volcanic rocks from the Southern Yidun.

Sample	Rb	Sr	$^{87}Sr/^{86}Sr$	±2σ	$^{87}Rb/^{86}Sr$	$(^{87}Sr/^{86}Sr)_i$	Sm	Nd	$^{143}Nd/^{144}Nd$	±2σ	$^{147}Sm/^{144}Nd$	$(^{143}Nd/^{144}Nd)_i$	$\varepsilon_{Nd}(t)$	T_{DM} (Ga)
DSG04-1	55.3	1100	0.706172	11	0.1455	0.7057	7.57	41.3	0.512407	8	0.1107	0.512248	−2.1	1.1
DSG07-1	31.5	1470	0.706063	12	0.0620	0.7059	5.79	33.1	0.51238	7	0.1057	0.512228	−2.5	1.1
DSG07-3-1	70.3	1190	0.706282	13	0.1709	0.7058	5.71	30.6	0.512389	21	0.1127	0.512227	−2.5	1.2
DSG07-3-2	23.1	1890	0.705993	7	0.0354	0.7059	5.40	31.9	0.512374	10	0.1023	0.512227	−2.5	1.1
DSG07-5	101	1120	0.706546	10	0.2609	0.7057	7.09	40.3	0.512438	5	0.1063	0.512285	−1.4	1.0
DSG07-7	140	987	0.707069	11	0.4104	0.7058	5.87	32.8	0.512373	12	0.1081	0.512217	−2.7	1.1
DSG07-8	88.8	1090	0.706584	14	0.2357	0.7059	5.76	34.1	0.512386	5	0.1021	0.512239	−2.3	1.0
DSG10-12	58.6	1570	0.706083	6	0.1080	0.7058	8.01	44.7	0.512439	3	0.1083	0.512283	−1.4	1.0
DSG10-13	47.1	2010	0.706009	4	0.0678	0.7058	6.55	38.3	0.512451	10	0.1033	0.512302	−1.0	1.0
DSG10-15	89.8	1020	0.706544	4	0.2547	0.7058	9.55	49.9	0.512432	3	0.1156	0.512266	−1.7	1.1
DSG10-2	131	1475	0.706616	7	0.2560	0.7058	9.28	56.9	0.512388	3	0.0985	0.512246	−2.1	1.0
DSG10-6	67.2	1845	0.706141	6	0.1054	0.7058	7.01	43.7	0.512489	5	0.0969	0.512349	−0.1	0.9
DSG10-7	35.3	1510	0.706069	5	0.0676	0.7059	7.13	44.7	0.512421	5	0.0964	0.512282	−1.4	1.0
LNT10-1	58.9	651	0.706586	5	0.2618	0.7058	7.23	41.7	0.512542	4	0.1048	0.512391	0.7	0.9
LNT10-3	52.6	1460	0.706348	5	0.1042	0.7060	6.49	37.4	0.512417	3	0.1048	0.512266	−1.7	1.0

Note: (1) $^{87}Rb/^{86}Sr$ and $^{147}Sm/^{144}Nd$ ratios are calculated using Rb, Sr, Sm and Nd contents (Table 7). (2) The $(^{87}Sr/^{86}Sr)_i$ and $\varepsilon_{Nd}(t)$ values are calculated at t = 220 Ma. (3) $\varepsilon_{Nd}(t)$ values are calculated using present-day $(^{147}Sm/^{144}Nd)_{CHUR} = 0.1967$ and $(^{143}Nd/^{144}Nd)_{CHUR} = 0.512638$; T_{DM} values are calculated using present-day $(^{147}Sm/^{144}Nd)_{DM} = 0.2137$ and $(^{143}Nd/^{144}Nd)_{DM} = 0.51315$.

of 2.2. Considering that the least discordant zircon provides the most robust initial $\varepsilon_{Hf}(t)$ values (Scherer et al., 2007), these positive $\varepsilon_{Hf}(t)$ values indicate that the zircons could be crystallized from relatively depleted magmas, whose positive $\varepsilon_{Nd}(t)$ values are in contrast with the negative $\varepsilon_{Nd}(t)$ values of the rocks derived from enriched magmas. A favorable interpretation would be that early zircons crystallized in the lower crust magma chamber, recorded the depleted nature of the magmas derived from the mantle source before the involvement of noticeable lower crust contamination. Moreover, a synthesis of zircon Hf isotopes and whole rock Nd isotopes demonstrates that it is the contamination by the lower crust that is likely to enrich the parental magma of volcanic rocks in the Southern Yidun arc.

In summary, several components were involved in the generation of the parental magmas of the volcanic rocks in the Southern Yidun arc (Fig. 14b), including slab-melt from subducting oceanic crust, melts from subducting sediments, slab-sediment-melt metasomatized mantle peridotite, and also components from lower crust by contamination, of which the lithospheric mantle is the dominant one; however, slab-melt from subducting oceanic crust gave some adakitic affinities to the volcanic rocks in the Southern Yidun arc.

5.4. Tectonic setting of the Yidun arc: a transition of island arc in the north to a continental arc in the south and its metallogenic implications

Through the petrology, geochemistry, and geochronology study of the volcanic rocks, mainly intermediate rocks such as trachyandesites in the Southern Yidun arc, and combined with previous studies on the arc-related volcanic rocks from Northern Yidun arc (e.g., Hou et al., 2003, 2007; Wang et al., 2013a,b), for the first time we are able to depict the whole picture of the tectonic scheme of the Yidun arc.

Temporally, zircon U–Pb ages of dacites and rhyolites in the Xiangcheng and Changtai regions of the Northern Yidun arc vary from ca. 228 Ma to 230 Ma (Wang et al., 2013a), which are ca. 8 to 10 million years older than the trachyandesites from this study in the Southern Yidun arc, proposing that subduction may be initiated in the Northern Yidun arc and extended to the southern part, rather than the other way suggested by Wang et al. (2013a).

Spatially, bimodal volcanic rocks are widespread in the Northern Yidun arc, while intermediate rocks take the majority in the southern part (Hou et al., 2003, 2007). The difference of spatial distribution of arc-related volcanic rocks between the northern and Southern Yidun arc suggests that they were probably generated under different arc settings, with the Northern Yidun arc similar to island arc and the Southern Yidun arc resembling continental arc.

The key factor that made the difference between the northern and southern parts of the Yidun arc could be the Zhongza Massif, which is situated in the west side of the Southern Yidun arc. The existence of this massif probably indicates that the Southern Yidun arc was developed on a basement of thickened continental crust. The crystallization of hornblende provides us with a clue to support this idea. A high water content of 3 to 4 wt.% is a prerequisite for hornblende crystallization in the pressure regime of lower crust and is often a characteristic of evolved magma through anhydrous silicate mineral crystallization in the arc system (Burnham, 1967, 1997; Richards, 2011; Richards et al., 2012). In the case of the Southern Yidun arc, persistent and intermittent replenishment and partial solidification of the magma chamber in the lower crust were likely to give rise to the high water content that enables the hornblende to crystallize. The stagnation of magma in the lower crust could be caused by flat-slab subduction as invoked by Hou et al. (2003); however, this could also be a result of the thickened continental crust above the subduction zone by the Zhongza Massif, compared with the Northern Yidun arc.

Moreover, this study also provides some hints of the origin of the Zhongza Massif in return. The Zhongza Massif was thought to be

Table 7
Whole-rock Pb isotopic data for Late Triassic volcanic rocks from the Southern Yidun.

Sample	Th	U	Pb	$^{206}Pb/^{204}Pb$	±2σ	$^{207}Pb/^{204}Pb$	±2σ	$^{208}Pb/^{204}Pb$	±2σ	$^{238}U/^{204}Pb$	$^{232}Th/^{204}Pb$	$(^{206}Pb/^{204}Pb)_t$	$(^{207}Pb/^{204}Pb)_t$	$(^{208}Pb/^{204}Pb)_t$
DSG07-5	14.5	3.71	29.0	18.247	1	15.604	1	38.444	3	8.10	32.7	17.966	15.590	38.086
DSG07-7	10.8	4.88	28.2	18.344	2	15.604	2	38.344	4	11.0	25.1	17.963	15.585	38.070
DSG04-1	14.2	2.63	32.7	18.172	3	15.606	3	38.371	7	5.08	28.4	17.995	15.597	38.061
DSG07-3-2-1	10.0	2.43	32.6	18.107	1	15.580	1	38.233	3	4.70	20.0	17.944	15.572	38.014
DSG07-3-2	13.0	2.98	45.5	18.078	1	15.584	1	38.223	3	4.13	18.6	17.935	15.577	38.019
DSG07-1	11.9	2.88	30.4	18.124	1	15.570	1	38.258	2	5.81	25.5	17.922	15.560	37.979
DSG07-8	15.5	3.06	19.6	18.331	3	15.619	2	38.650	6	9.93	52.0	17.986	15.602	38.081

Note: (1) $^{238}U/^{204}Pb$ and $^{232}Th/^{204}Pb$ ratios are calculated by using measured whole-rock U, Th and Pb contents (Table 7) and present-day whole-rock Pb isotopic ratios. (2) Initial Pb isotopic ratios are calculated at t = 220 Ma by using single-stage Pb isotopic evolution model.

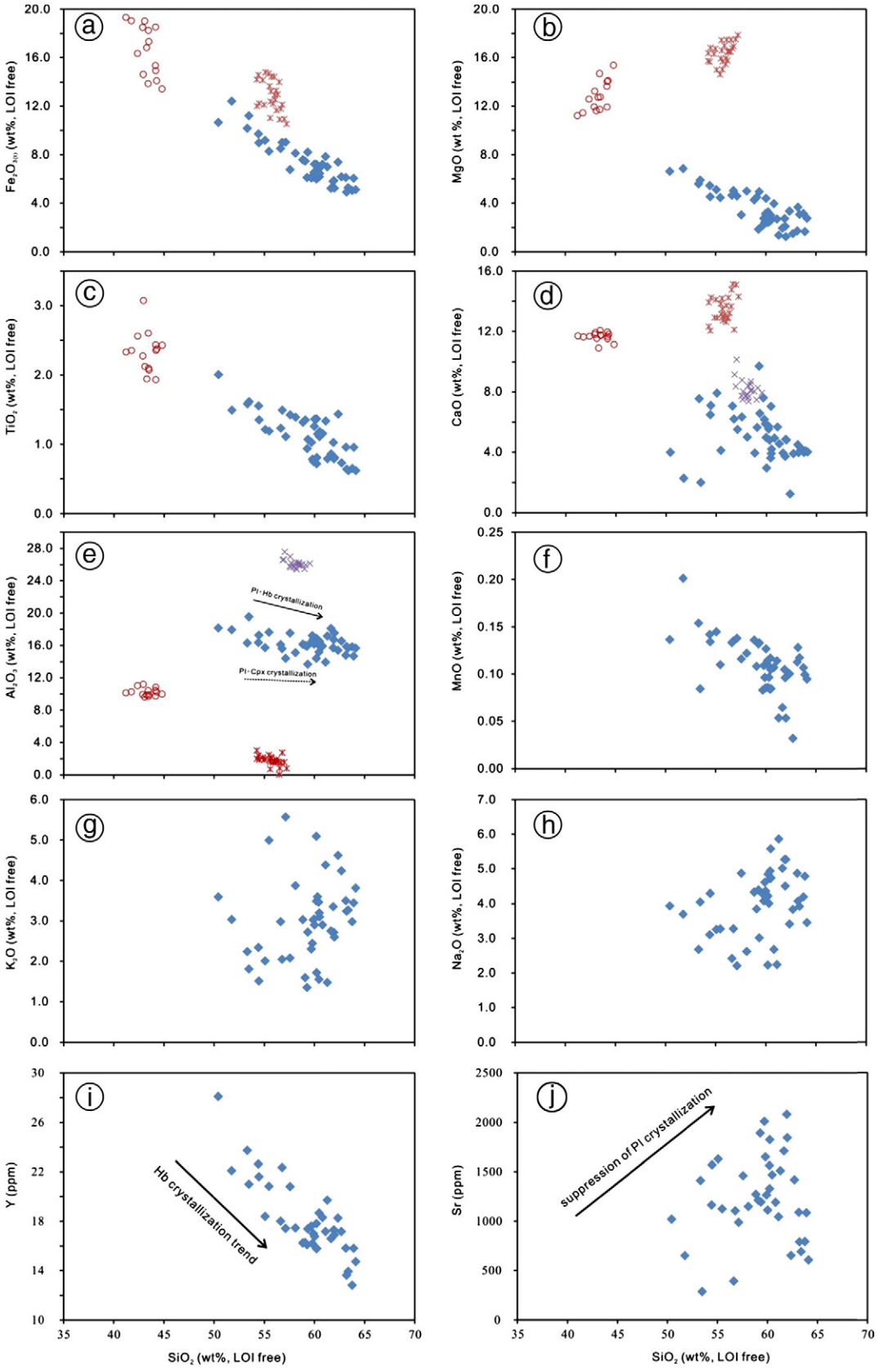

Fig. 8. Harker diagrams of selected major and trace elements vs. SiO_2 contents for the Southern Yidun volcanic rocks (diamond), clinopyroxene (asterisk), hornblende (circle), and plagioclase (×) from these volcanic rocks.

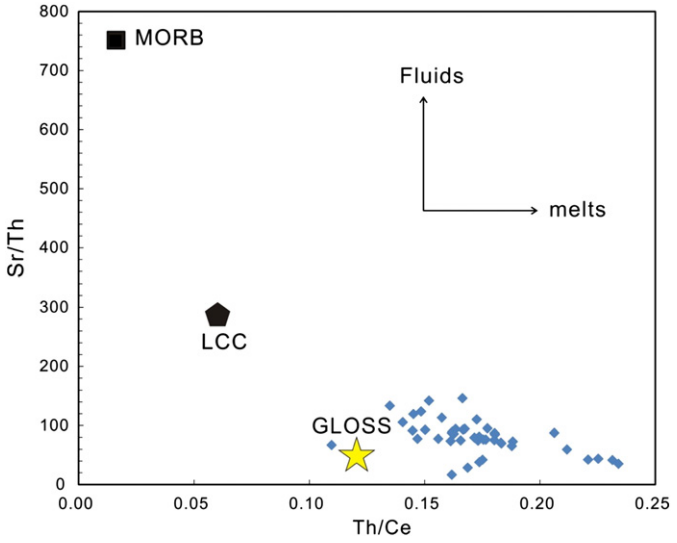

Fig. 9. Plot of Th/Ce vs. Sr/Th for the Southern Yidun volcanic rocks. For comparison, the estimated composition of normal mid-ocean ridge basalt (N-MORB, from Sun and McDonough, 1989), Lower Continental Crust (LCC, from Rudnick and Gao, 2003), and global subducting sediment (GLOSS, from Plank and Langmuir, 1998) are also plotted.

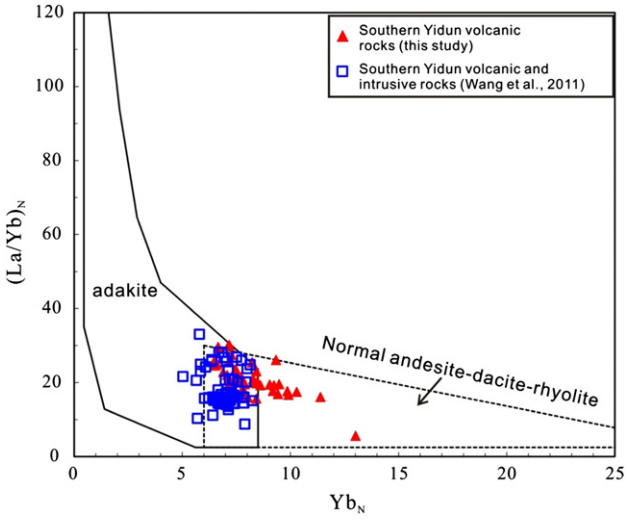

Fig. 11. Plot of $(La/Yb)_N$ vs. Yb_N (after Martin, 1999) for the Southern Yidun volcanic rocks.

derived from the Yangtze Block, based on the similarities of the stratigraphic sequences and the fossil assemblages of this massif to those in the Longmen Shan Thrust Nappe Belt (Chang, 1997; Reid et al., 2007). In this study, our newly obtained U–Pb ages and Hf isotopic compositions of those inherited zircons from the Southern Yidun volcanic rocks could provide further constraints on the history of this basement beneath the Southern Yidun Arc, because those inherited zircons could be scavenged from the basement rocks by the parental magma of the Southern Yidun volcanic rocks during its ascent. All U–Pb dating ages of zircons from the Southern Yidun volcanic rocks in this study are plotted in Fig. 13. Detrital zircon dating results from Late Triassic sandstones in the Yidun Group in the Southern Yidun arc are also shown for comparison. It is shown that there are roughly four age populations from both dataset, with ranges of 196–236 Ma (n = 51), 816–936 Ma (n = 4), 1449–1675 Ma (n = 5), and 2354–2589 Ma (n = 5), respectively (Fig. 13). It was reported that some inherited zircons with ages of even over 2300 Ma have been discovered in pegmatite from the Zhongza Massif (Reid et al., 2007). The ca. 1500 Ma age group probably represents one Mesoproterozoic magmatic event, which has been recently identified in the southwestern Yangtze Block (e.g., Zhao et al., 2010 and references therein). The 810–930 Ma ages are similar to the timing of extensive Neoproterozoic magmatism within the western Yangtze Block (Li et al., 2003; Xiao et al., 2007; Zheng et al., 2006; Zhou et al., 2002). Various ages of inherited zircons from the volcanic rocks of the Southern Yidun arc reveal that the basement rocks beneath the Southern Yidun arc could have been reworked by multiple magmatic activities from Paleoproterozoic to Late Triassic. In addition, magmatic zircons (ca. 220 Ma) have uniform initial Hf compositions with most $\varepsilon_{Hf}(t)$ values varying from 0 to 4.0 and T_{DM1} model ages varying from 700 Ma to 900 Ma. However, the inherited zircons from the Zhongdian volcanic rocks have variable initial Hf compositions with negative $\varepsilon_{Hf}(t)$ values and nearly concordant U–Pb ages varying from 252 Ma to 2589 Ma. If we assume that these inherited zircons came from the Zhongza Massif, then the consistency of the ages of the inherited zircons with the various magmatic events within the Yangtze Block indicates that the Zhongza Massif was derived from the Yangtze Block, no earlier than ca. 400 Ma (Fig. 13).

Different types of ore deposits usually show their preferences for certain tectonic settings. Recognition of the nature of the northern and Southern Yidun arcs provides us with a very good chance to examine the variation of ore deposit types with different arc settings. In the north Yidun arc that used to be an island arc, a bunch of VMS deposits occurred (Fig. 14a); while in the Southern Yidun arc where a continental arc was developed, several porphyry deposits were developed (Fig. 14b). Thus, our interpretation of the paleotectonic setting agrees well with the distribution of different types of ore deposits in the Yidun arc.

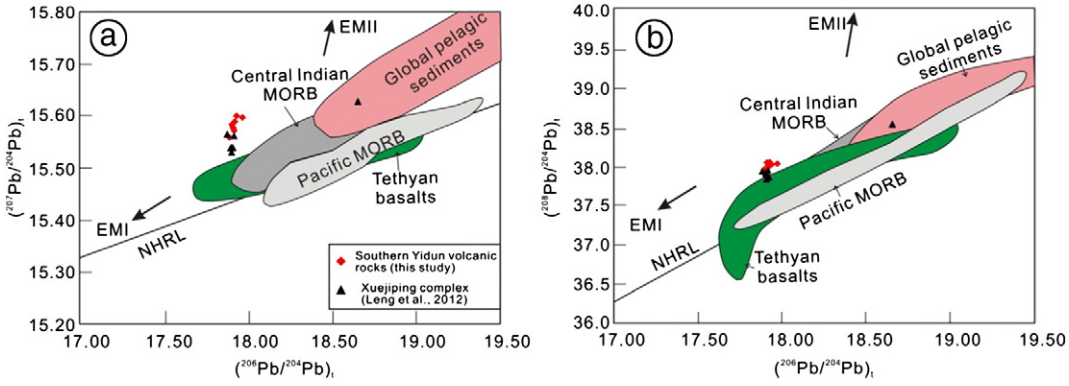

Fig. 10. Plots of initial $^{207}Pb/^{204}Pb$ vs. $^{206}Pb/^{204}Pb$ (a), and $^{208}Pb/^{204}Pb$ vs. $^{206}Pb/^{204}Pb$ (b) diagrams for the Southern Yidun volcanic rocks. The fields of global pelagic sediments, central Indian MORB, Pacific MORB, and Tethyan basalts are from Fan et al. (2010). DMM, HIUM and EMII represent three types of mantle end-members of Zindler and Hart (1986). NHRL represents Northern Hemisphere reference line of Hart (1984).

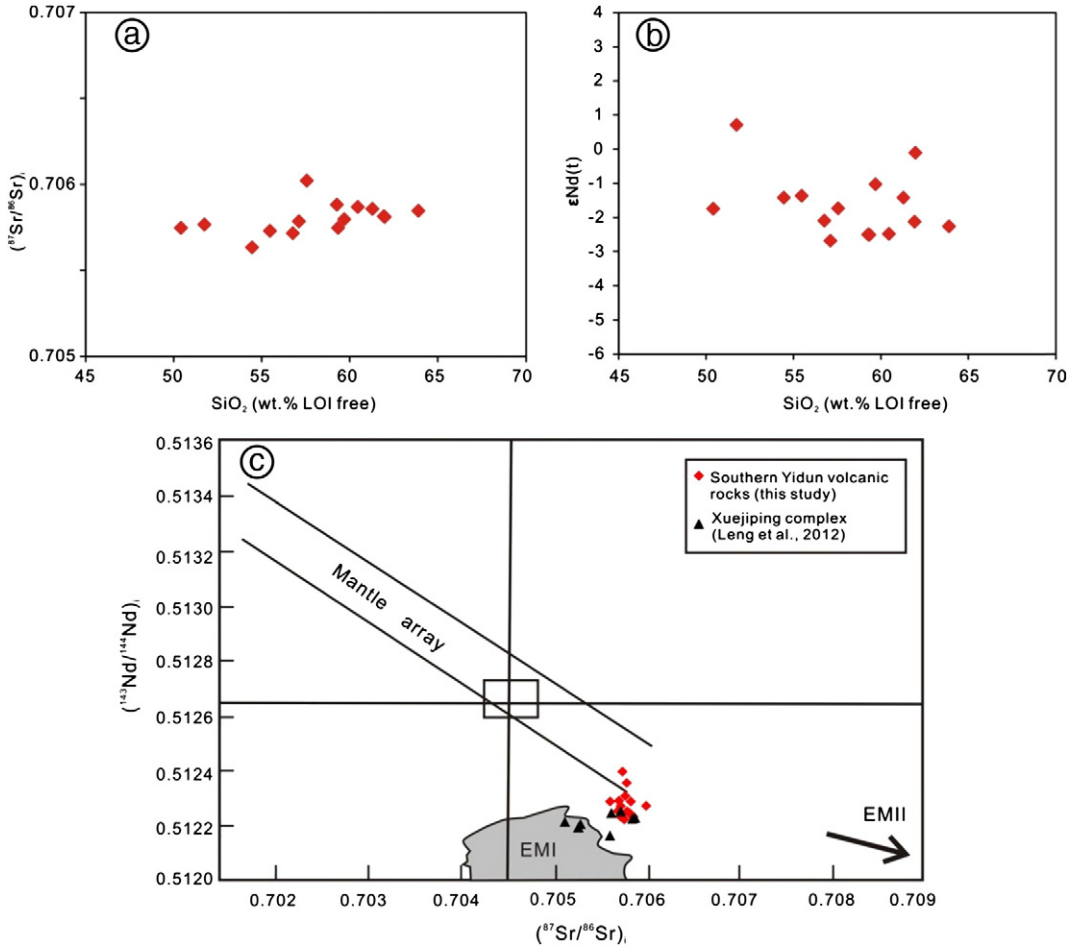

Fig. 12. Diagrams of initial $^{87}Sr/^{86}Sr$ vs. SiO_2 (a), and $\varepsilon_{Nd}(t)$ vs. SiO_2 (b), and $(^{143}Nd/^{144}Nd)_i$ vs. $(^{87}Sr/^{86}Sr)_i$ (c) diagrams of the Southern Yidun volcanic rocks. The Sr–Nd data of Xuejiping complex from Leng et al. (2012) are also plotted for comparison.

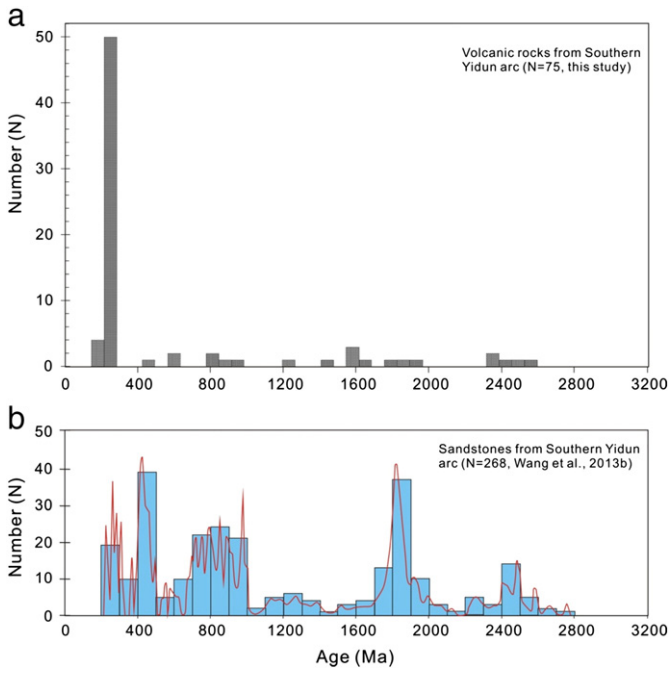

Fig. 13. Histogram of $^{206}Pb/^{238}U$ ages for zircons from the Late Triassic volcanic rocks in the Southern Yidun arc (a). The U–Pb age spectra of detrital zircons from Late Triassic sandstone in the Southern Yidun arc (b, from Wang et al., 2013b) are presented here for comparison.

6. Conclusions

We draw the following conclusions based on our combined studies of zircon U–Pb ages and Hf isotopes, whole-rock geochemistry and Sr–Nd–Pb isotopes, and mineralogical data for the Late Triassic volcanic rocks in the Southern Yidun arc.

(1) SIMS and LA–ICP-MS zircon U–Pb dating results indicate that these Late Triassic volcanic rocks, which are mainly composed of trachyandesites, were erupted at ca. 220 Ma. These volcanic rocks are enriched in LILEs, but depleted in Nb, Ta and Ti, resembling the normal arc magmas, which indicates that they are associated with arc magmatism. The hornblende geobarometer suggests that the magma had stagnated in the lower crust (~19 km), where hornblende crystallized while plagioclase crystallization was suppressed, giving rise to high Sr/Y ratios. Moreover, the steeply right-declined REE pattern suggests adakitic affinity of these volcanic rocks.

(2) The trace element geochemical and isotopic characteristics suggest that several components were involved in the generation of the parental magmas of the volcanic rocks in the Southern Yidun arc, including slab-melt from subducting oceanic crust, melts from subducting sediments, slab-sediment-melt metasomatized mantle peridotite, and also components from lower crust by contamination, of which the lithospheric mantle is the dominant one.

(3) In combination with previous studies on the Northern Yidun arc, we suggest that the Southern Yidun arc was a continental arc

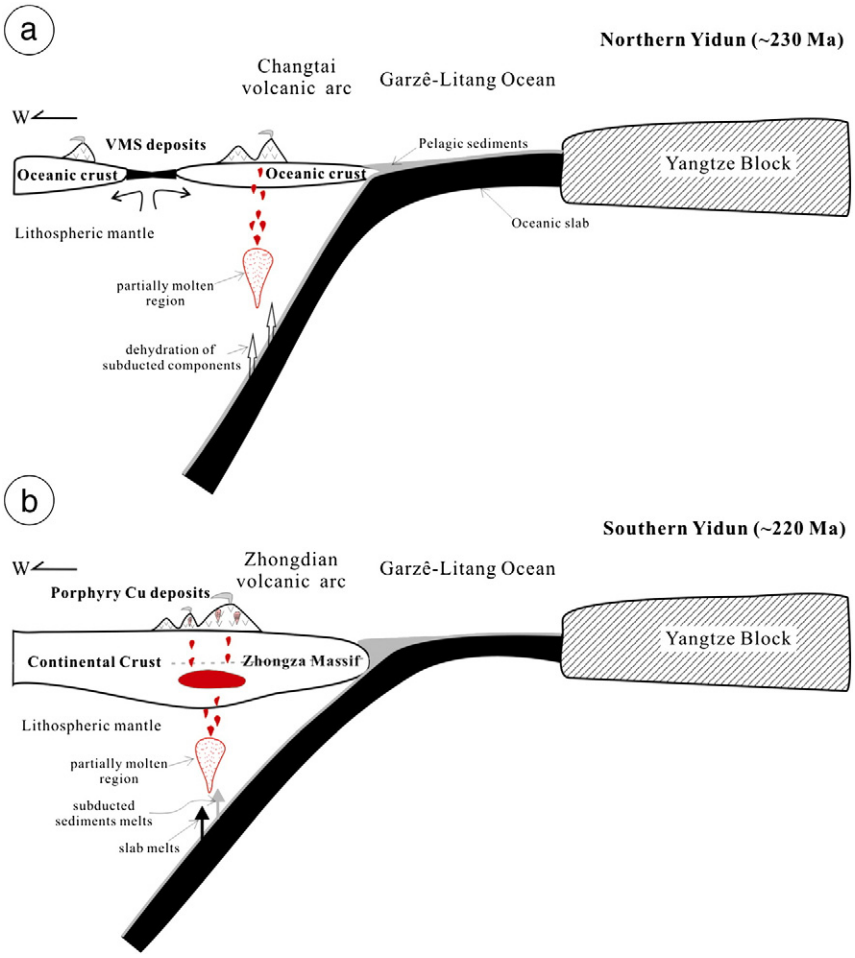

Fig. 14. Schematic model of the tectonic setting and metallogenesis of the Yidun arc, highlighting the difference between its northern part (a, Changtai arc) and the southern part (b, Zhongdian arc). Based on our study on the Southern Yidun arc and previous work on the Northern Yidun arc (e.g., Hou et al., 2003, 2004; Wang et al., 2013a,b), we interpret that the Southern Yidun arc is a continental arc, while the Northern Yidun is an island arc. See text for discussion.

and the Northern Yidun arc resembled an island arc, probably as a result of the situation of the Zhongza Massif that has thickened the continental crust in the Southern Yidun arc. The thickened continental crust enabled magma evolution in a lower crust magma chamber which fertilized porphyries that host a bunch of copper mineralization in the same arc belt as the volcanic rocks in this study also source from.

Acknowledgments

Author C.B. Leng highly appreciates David Cooke, Lejun Zhang, Wei Hong, Chun Kit Lai, and Khin Zaw for their support and help during his six-month visit at CODES, University of Tasmania, Australia. We would like to thank Chaozhi Yang, Waiquan Wang, Xiaomin Cao, and Xiangdong Zhao for their help and fruitful discussion during field investigation. In addition, many thanks are due to Xianhua Li, Qiuli Li, Guoqiang Tang, Zhaochu Hu, Liang Li, Jinhui Yang, Yueheng Yang, Jianyong Cui, Wenqin Zheng, Shirong Liu, and Guofu Zhou for their assistance in geochemical and isotope analyses. Many thanks are due especially to Yann Rolland and one anonymous reviewer who helped with careful reviews of the text. The Editor-in-Chief Nelson Eby is also appreciated for his helpful suggestions. This study was jointly supported by grants from the 12th Five-Year Plan project of State Key Laboratory of Ore-deposit Geochemistry, Chinese Academy of Sciences (SKLODG-ZY125-03), the Natural Science Foundation of China (41373051, 41003023, 40873039), and the Science and Technology Foundation of Guizhou Province (Grant No. [2011]2355).

Appendix A

Supplementary data to this article can be found online at http://dx.doi.org/10.1016/j.lithos.2013.12.018.

References

Ayers, J., 1998. Trace element modeling of aqueous fluid–peridotite interaction in the mantle wedge of subduction zones. Contributions to Mineralogy and Petrology 132, 390–404.
Ben Othman, D., White, W.M., Patchett, J., 1989. The geochemistry of marine sediments, island arc magma genesis, and crust–mantle recycling. Earth and Planetary Science Letters 94, 1–21.
Blichert-Toft, J., Albarede, F., 1997. The Lu–Hf geochemistry of chondrites and the evolution of the mantle–crust system. Earth and Planetary Science Letters 148, 243–258.
Boynton, W.V., 1984. Geochemistry of the rare earth elements: meteorite studies. In: Henderson, P. (Ed.), Rare Earth Element Geochemistry. Elsevier, pp. 63–114.
Burchfiel, B.C., Chen, Z., Liu, Y., Royden, L.H., 1995. Tectonics of the Longmen Shan and adjacent regions, central China. International Geology Review 37, 661–735.
Burnham, C.W., 1967. Hydrothermal fluids at the magmatic stage, In: Barnes, H.L. (Ed.), Geochemistry of Hydrothermal Ore Deposits, First edition. Wiley, New York, pp. 34–76.
Burnham, C.W., 1997. Magmas and hydrothermal fluids, In: Barnes, H.L. (Ed.), Geochemistry of Hydrothermal Ore Deposits, Third edition. Wiley, New York, pp. 63–123.
Chang, C.F., 1997. Geology and Tectonics of Qinghai–Xizang Plateau. Science Press, Beijing 1–153.
Chen, B., Wang, K., Liu, W., Cai, Z., Zhang, Q., Peng, X., Qiu, Y., Zheng, Y., 1987. Geotectonic of the Nujiang–Lancangjiang–Jinshajiang Region. Geological Publishing House, Beijing 1–204 (in Chinese).
Defant, M.J., Drummond, M.S., 1990. Derivation of some modern arc magmas by melting of young subducted lithosphere. Nature 347, 662–665.
Drummond, M.S., Defant, M.J., 1990. A model for trondhjemite–tonalite–dacite genesis and crustal growth via slab melting: Archaean to modern comparisons. Journal of Geophysical Research 95, 21503–21521.

Fan, W.M., Wang, Y.J., Zhang, A.M., Zhang, F.F., Zhang, Y.Z., 2010. Permian arc–back-arc basin development along the Ailaoshan tectonic zone: geochemical, isotopic and geochronological evidence from the Mojiang volcanic rocks, Southwest China. Lithos 119, 553–568.
Griffin, W.L., Wang, X., Jackson, S.E., Pearson, N.J., O'Reilly, S.Y., Xu, X., Zhou, X., 2002. Zircon chemistry and magma mixing, SE China: in-situ analysis of Hf isotopes, Tonglu and Pingtan igneous complexes. Lithos 61, 237–269.
Grifin, W.L., Pearson, N.J., Belousova, E.A., Saced, A., 2006. Comment: Hf-isotope heterogeneity in zircon 91500. Chemical Geology 233, 358–363.
Hart, S.R., 1984. A large-scale isotope anomaly in the Southern Hemisphere mantle. Nature 309, 753–757.
Hastie, A.R., Kerr, A.C., Pearce, J.A., Mitchell, S.F., 2007. Classification of altered volcanic island arc rocks using immobile trace elements: development of the Th–Co discrimination diagram. Journal of Petrology 48, 2341–2357.
Hawkesworth, C.J., Turner, S.P., McDermott, F., Peate, D.W., Van Calsteren, P., 1997. U–Th isotopes in arc magmas: implications for element transfer from the subducted crust. Science 276, 551–555.
Hollister, L.S., Grisson, G.C., Peters, E.K., Stowell, H.H., Sisson, V.B., 1987. Confirmation of the empirical correlation of Al in hornblende with pressure of solidification of calc-alkaline plutons. American Mineralogists 72, 231–239.
Hou, Z.Q., 1993. The tectono-magmatic evolution of Yidun island-arc and geodynamic setting of the formation of Kuroko-type massive sulphide deposits in Sanjiang region, southwestern China. Resource Geology 17, 336–350.
Hou, Z.Q., Luo, Z.W., 1992. Origin of the andesite in Yidun island arc, Sanjiang region. Acta Petrologica et Mineralogica 11, 1–14 (in Chinese with English abstract).
Hou, Z.Q., Mo, X.X., 1991. The evolution of Yidun island-arc and implications in the exploration of Kuroko-type volcanogenic massive sulphide deposits in Sanjiang area, China. Earth Science-Journal of China University of Geosciences 16, 153–164 (in Chinese with English abstract).
Hou, Z.Q., Yang, Y.Q., Wang, H.P., Qu, X.M., Lü, Q.T., Huang, D.H., Wu, X.Z., Tang, S.H., Zhao, J.H., 2003. Collision-orogenic Progress and Mineralization System of Yidun arc. Geological Publishing House, Beijing 1–345 (in Chinese).
Hou, Z.Q., Yang, Y.Q., Qu, X.M., Huang, D.H., Lü, Q.T., Wang, H.P., Yu, J.J., Tang, S.H., 2004. Tectonic evolution and mineralization systems of the Yidun arc orogen in Sanjiang region, China. Acta Geologica Sinica 78, 109–119 (in Chinese with English abstract).
Hou, Z., Zaw, K., Pan, G., Mo, X., Xu, Q., Hu, Y., Li, X., 2007. Sanjiang Tethyan metallogenesis in SW China: tectonic setting, metallogenic epochs and deposit types. Ore Geology Reviews 31, 48–87.
Jian, P., Liu, D., Kroener, A., Zhang, Q., Wang, Y., Sun, X., Zhang, W., 2009. Devonian to Permian plate tectonic cycle of the Paleo-Tethys Orogen in southwest China (I): geochemistry of ophiolites, arc/back-arc assemblages and within-plate igneous rocks. Lithos 113, 748–766.
Leake, B.E., Woolley, A.R., Arps, C.E.S., Birch, W.D., Gilbert, M.C., Grice, J.D., Hawthorne, F.C., Kato, A., Kisch, H.J., Krivovichev, V.G., Linthout, K., Laird, J., Mandarino, J., Maresch, W.V., Nickel, E.H., Rock, N.M.S., Schumacher, J.C., Smith, D.C., Stephenson, N.C.N., Ungaretti, L., Whittaker, E.J.W., Youzhi, G., 1997. Nomenclature of amphiboles: report of the Subcommittee on Amphiboles of the International Mineralogical Association Commission on new minerals and mineral names. Mineralogical Magazine 61, 295–321.
Leng, C.B., Zhang, X.C., Hu, R.Z., Wang, S.X., Zhong, H., Wang, W.Q., Bi, X.W., 2012. Zircon U–Pb and molybdenite Re–Os geochronology and Sr–Nd–Pb–Hf isotopic constraints on the genesis of the Xuejiping porphyry copper deposit in Zhongdian, Northwest Yunnan, China. Journal of Asian Earth Sciences 60, 31–48.
Li, X., Liu, W., Wang, Y., Zhu, Q., Du, D., Shen, G., Liu, C., Que, M., Yang, S., Li, D., Feng, Q., 1999. The Tectonic Evolution and Metallogenesis in the Tethys of the Nujiang–Lancangjiang–Jinshajiang Area, South-Western China. Geological Publishing House, Beijing 1–276 (in Chinese).
Li, X.H., Li, Z.X., Ge, W.C., Zhou, H.W., Li, W.X., Liu, Y., Wingate, M.T.D., 2003. Neoproterozoic granitoids in South China: crustal melting above a mantle plume at ca. 825 Ma? Precambrian Research 122, 45–83.
Li, X.H., Liu, Y., Li, Q.L., Guo, C.H., Chamberlain, K.R., 2009. Precise determination of Phanerozoic zircon Pb/Pb age by multicollector SIMS without external standardization. Geochemistry, Geophysics, Geosystems 10, Q04010. http://dx.doi.org/10.1029/2009GC002400.
Li, W.C., Zeng, P.S., Hou, Z.Q., White, N.C., 2011. The Pulang porphyry copper deposit and associated felsic intrusions in Yunnan Province, southwest China. Economic Geology 106, 79–92.
Liu, Y.S., Hu, Z.C., Gao, S., Günther, D., Xu, J., Gao, C.G., Chen, H.H., 2008. In situ analysis of major and trace elements of anhydrous minerals by LA–ICP-MS without applying an internal standard. Chemical Geology 257, 34–43.
Liu, Y., Gao, S., Hu, Z., Gao, C., Zong, K., Wang, D., 2010a. Continental and oceanic crust recycling-induced melt-peridotite interactions in the Trans-North China Orogen: U–Pb dating, Hf isotopes and trace elements in zircons of mantle xenoliths. Journal of Petrology 51, 537–571.
Liu, Y., Hu, Z., Zong, K., Gao, C., Gao, S., Xu, J., Chen, H., 2010b. Reappraisement and refinement of zircon U–Pb isotope and trace element analyses by LA–ICP-MS. Chinese Science Bulletin 55, 1535–1546.
Ludwig, K.R., 2003. ISOPLOT 3.00: a Geochronological Toolkit for Microsoft Excel. Berkeley Geochronology Center, Berkeley, California.
Martin, H., 1999. Adakitic magmas: modern analogues of Archaean granitoids. Lithos 46, 411–429.
Martin, H., Smithies, R.H., Rapp, R., Moyen, J.F., Champion, D., 2005. An overview of adakite, tonalite–trondhjemite–granodiorite (TTG), and sanukitoid: relationships and some implications for crustal evolution. Lithos 79, 1–24.
Metcalfe, I., 1996. Gondwanaland dispersion, Asian accretion and evolution of eastern Tethys. Australian Journal of Earth Sciences 43, 605–623.
Metcalfe, I., 2006. Paleozoic and Mesozoic tectonic evolution and paleogeography of East Asian crustal fragments: the Korean Peninsula in context. Gondwana Research 9, 24–46.
Mo, X.X., Lu, F.X., Shen, S.Y., Zhu, Q.W., Hou, Z.Q., 1993. Volcanism and Metallogeny in the Sanjiang Tethys. Geological Publishing House, Beijing 1–250 (in Chinese with English abstract).
Mo, X.X., Hou, Z.Q., Niu, Y.L., Dong, G.C., Qu, X.M., Zhao, Z.D., Yang, Z.M., 2007. Mantle contributions to crustal thickening during continental collision: evidence from Cenozoic igneous rocks in southern Tibet. Lithos 96, 225–242.
Nowell, G.M., Kempton, P.D., Noble, S.R., Fitton, J.G., Sauders, A.D., Mahoney, J.J., Taylor, R.N., 1998. High precision Hf isotope measurements of MORB and OIB by thermal ionization mass spectrometry: insights into the depleted mantle. Chemical Geology 149, 211–233.
Pearce, J.A., 1996. A user's guide to basalt discrimination diagrams. In: Wyman, D.A. (Ed.), Trace Element Geochemistry of Volcanic Rocks: Applications for Massive Sulphide Exploration. Short Course Notes, 12. Geological Association of Canada, pp. 79–113.
Pearce, J.A., Peate, D.W., 1995. Tectonic implications of the composition of volcanic arc magmas. Annual Review of Earth and Planetary Sciences 23, 251–286.
Plank, T., Langmuir, C.H., 1998. The chemical composition of subducting sediment and its consequences for the crust and mantle. Chemical Geology 145, 325–394.
Qi, L., Hu, J., Gregoire, D.C., 2000. Determination of trace elements in granites by inductively coupled plasma mass spectrometry. Talanta 51, 507–513.
Qu, X.M., Hou, Z.Q., Zhou, S.G., 2002. Geochemical and Nd, Sr isotopic study of the post-orogenic granites in the Yidun arc belt of northern Sanjiang region, southwestern China. Resource Geology 52, 163–172.
Rapp, R.P., Shimizu, N., Norman, M.D., Applegate, G.S., 1999. Reaction between slab-derived melts and peridotite in the mantle wedge: experimental constraints at 3.8 GPa. Chemical Geology 160, 335–356.
Reid, A.J., Wilson, C.J.L., Liu, S., 2005. Structural evidence for the Permo-Triassic tectonic evolution of the Yidun Arc, eastern Tibetan plateau. Journal of Structural Geology 27, 119–137.
Reid, A., Wilson, C.J.L., Shun, L., Pearson, N., Belousova, E., 2007. Mesozoic plutons of the Yidun Arc, SW China: U/Pb geochronology and Hf isotopic signature. Ore Geology Reviews 31, 88–106.
Ren, S.K., Zhang, X.C., Yang, C.Z., 2001. Excusion guide Zhongdian porphyry Cu–Au district. Yunnan Gaoshan Exploration and Development Co. Ltd., pp. 1–33. (Unpublished exploration report).
Richards, J.P., 2011. High Sr/Y arc magmas and porphyry Cu ± Mo ± Cu deposits: just add water. Economic Geology 106, 1075–1081.
Richards, J.P., Spell, T., Rameii, E., Razique, A., Fletcher, T., 2012. High Sr/Y magmas reflect arc maturity, high magmatic water content, and porphyry Cu ± Mo ± Au potential: examples from the Tethyan arcs of central and eastern Iran and western Pakistan. Economic Geology 107, 295–332.
Roger, F., Jolivet, M., Malavieille, J., 2010. The tectonic evolution of the Songpan-Garzê (North Tibet) and adjacent areas from Proterozoic to Present: a synthesis. Journal of Asian Earth Sciences 39, 254–269.
Rohrlach, B.D., Loucks, R.R., 2005. Multi-million-year cyclic ramp-up of volatiles in a lower crustal magma reservoir trapped below the Tampakan copper–gold deposit by Mio-Pliocene crustal compression in the southern Philippines. In: Porter, T.M. (Ed.), Super Porphyry Copper & Gold Deposits—a Global Perspective, v2. PCG Publishing, Adelaide, pp. 269–407.
Rollinson, H.R., 1993. Using Geochemical Data: Evaluation, Presentation, Interpretation. Longman, London 1–352.
Rudnick, R.L., Gao, S., 2003. Composition of the continental crust. In: Rudnick, R.L. (Ed.), Treatise on Geochemistry. Elsevier, pp. 1–64.
Scherer, E., Munker, C., Mezger, K., 2001. Calibration of the lutetium–hafnium clock. Science 193, 683–687.
Scherer, E.E., Whitehouse, M.J., Munker, C., 2007. Zircon as a monitor of crustal growth. Elements 3, 19–24.
Sengör, A.M.C., 1985. Tectonic subdivisions and evolution of Asia. Bulletin of the Technical University of Istanbul 46, 355–435.
Song, X.Y., Zhou, M.F., Cao, Z.M., Robinson, P.T., 2004. Late Permian rifting of the South China Craton caused by the Emeishan mantle plume? Journal of the Geological Society 161, 773–781.
Sun, S.S., McDonough, W.F., 1989. Chemical and isotopic systematics of oceanic basalts: implications for mantle composition and processes. In: Saunders, A.D., Norry, M.J. (Eds.), Magmatism in the Ocean Basins. Geological Society London Special Publications, 42, pp. 313–345.
Tatsumi, Y., Hamilton, D.L., Nesbitt, R.W., 1986. Chemical characteristics of fluid phase released from a subducted lithosphere and origin of arc magmas: evidence from high-pressure experiments and natural rocks. Journal of Volcanology and Geothermal Research 29, 293–309.
Vervoort, J.D., Blichert-Toft, J., 1999. Evolution of the depleted mantle: Hf isotope evidence from juvenile rocks through time. Geochimica et Cosmochimica Acta 63, 533–556.
Wang, E., Burchfiel, B.C., 2000. Late Cenozoic to Holocene deformation in southwestern Sichuan and adjacent Yunnan, China, and its role in formation of the southeastern part of the Tibetan Plateau. In: Geissman John, W., Glazner Allen, F. (Eds.), Special Focus on the Himalaya. Geological Society of America Bulletin, Boulder, CO, United States, pp. 413–423.
Wang, X.F., Metcalfe, I., Jian, P., He, L.Q., Wang, C.S., 2000. The Jinshajiang–Ailaoshan Suture Zone, China: tectonostratigraphy, age and evolution. Journal of Asian Earth Sciences 18, 675–690.
Wang, B.Q., Zhou, M.F., Li, J.W., Yan, D.P., 2011. Late Triassic porphyritic intrusions and associated volcanic rocks from the Shangri-La region, Yidun terrane, Eastern Tibetan Plateau: adakitic magmatism and porphyry copper mineralization. Lithos 127, 24–38.

Wang, B.Q., Zhou, M.F., Chen, W.T., Gao, J.F., Yan, D.P., 2013a. Petrogenesis and tectonic implications of the Triassic volcanic rocks in the northern Yidun Terrane, Eastern Tibet. Lithos 175–176, 285–301.

Wang, B.Q., Wang, W., Chen, W.T., Gao, J.F., Zhao, X.F., Yan, D.P., Zhou, M.F., 2013b. Constraints of detrital zircon U–Pb ages and Hf isotopes on the provenance of the Triassic Yidun Group and tectonic evolution of the Yidun Terrane, Eastern Tibet. Sedimentary Geology 289, 74–98.

Wiedenbeck, M., Alle, P., Corfu, F., Griffin, W.L., Meier, M., Oberli, F., Quadt, A.V., Roddick, J.C., Spiegel, W., 1995. Three natural zircon standards for U–Th–Pb, Lu–Hf, trace element and REE analyses. Geostandards and Geoanalytical Research 19, 1–23.

Woodhead, J.D., Hergt, J.M., 2005. A preliminary appraisal of seven natural zircon reference materials for in situ Hf-isotope analysis. Geostandards and Geoanalytical Research 29, 183–195.

Wu, F.Y., Yang, Y.H., Xie, L.W., Yang, J.H., Xu, P., 2006. Hf isotopic compositions of the standard zircons and baddeleyites used in U–Pb geochronology. Chemical Geology 234, 105–126.

Xiao, L., Zhang, H.F., Clemens, J.D., Wang, Q.W., Kan, Z.Z., Wang, K.M., Ni, P.Z., Liu, X.M., 2007. Late Triassic granitoids of the eastern margin of the Tibetan Plateau: geochronology, petrogenesis and implications for tectonic evolution. Lithos 96, 436–452.

Xu, Z., Hou, L., Wang, Z., 1992. Orogenic Processes of the Songpan–Garzê Orogenic Belt of China. Geological Publishing House, Beijing 1–190 (in Chinese).

Yin, A., Harrison, T.M., 2000. Geologic evolution of the Himalayan–Tibetan orogen. Annual Review of Earth and Planetary Sciences 28, 211–280.

Yunnan Bureau of Geology and Mineral Resources (YBGMR), 1999. Yunnan Geological Map series in scale of 1: 50000: Qiansui Sheet (H47E023016) and Hongshan Sheet (H47E024016) (in Chinese).

Yunnan Bureau of Geology and Mineral Resources (YBGMR), 1990. Regional Geology of Yunnan Province. Geological Publishing House, Beijing 1–728 (in Chinese with English abstract).

Zeng, P.S., Mo, X.X., Yu, X.H., Hou, Z.Q., Xu, Q.D., Wang, H.P., Li, H., Yang, C.Z., 2003. Porphyries and porphyry copper deposits in Zhongdian area, Northwest Yunnan. Mineral Deposits 20, 393–400 (in Chinese with English abstract).

Zhang, N., Cao, Y., Lio, Y.A., Zhao, Y., Zhang, H., Hu, D., Zhang, R., Wang, L., 1998. Geology and Metallogeny in the Garzê–Litang Rift Zone. Geological Publishing House, Beijing 1–119 (in Chinese).

Zhao, X.F., Zhou, M.F., Li, J.W., Sun, M., Gao, J.F., Sun, W.H., Yang, J.H., 2010. Late Paleoproterozoic to early Mesoproterozoic Dongchuan Group in Yunnan, SW China: implications for tectonic evolution of the Yangtze Block. Precambrian Research 182, 57–69.

Zheng, J.P., Griffin, W.L., O'Reilly, S.Y., Zhang, M., Pearson, N., Pan, Y.M., 2006. Widespread Archean basement beneath the Yangtze craton. Geology 34, 417–420.

Zhong, D., 2000. Palaeotethysides in West Yunnan and Sichuan. China. Science Press, Beijing 1–248.

Zhou, D., Graham, S.A., 1996. The Songpan–Ganzi complex of the west Qinling Shan as a Triassic remnant ocean basin. In: Yin, A., Harrison, M. (Eds.), The Tectonic Evolution of Asia. Cambridge University Press, Cambridge, pp. 281–299.

Zhou, M.F., Yan, D.P., Kennedy, A.K., Li, Y.Q., Ding, J., 2002. SHRIMP U–Pb zircon geochronological and geochemical evidence for Neoproterozoic arc-magmatism along the western margin of the Yangtze Block, South China. Earth and Planetary Science Letters 196, 51–67.

Zi, J.W., Cawood, P.A., Fan, W.M., Wang, Y.J., Tohver, E., McCuaig, T.C., Peng, T.P., 2012. Triassic collision in the Paleo-Tethys Ocean constrained by volcanic activity in SW China. Lithos 144–145, 145–160.

Zindler, A., Hart, S., 1986. Chemical geodynamics. Annual Review of Earth and Planetary Sciences 14, 493–571.